Impacts of fractional and fractal differential operators in applied sciences

by

Professor Emile Franc Doungmo Goufo

Department of Mathematical Sciences, University of South Africa, Florida, 0003 South Africa.

Abstract

There are still many phenomena that occur in applied sciences and remain fully or partly unexplained. Some of them are related to auto-replication, self-similarity or self-organization processes. However, they remain fascinating in sciences, engineering and technology as their applications have been widely used to describe number of outstanding science problems. Finding innovative techniques capable of generating some of these processes in various fields has then become the priority for number of scientists. Some of these fields includes chaos theory, wave motion, rock fracture, and neuron science. In this paper, we combine some recent mathematical concepts to model and generate some fractal processes happening in real life and useful in applied sciences. To achieve it, we use systems of differential equations together with recently developed fractal and fractional operators. The impacts of these operators in the different systems used are remarkable and concur with the expected results. Numerical simulations are performed and show that the new systems are involved in various types of fractal dynamics with the replication of the initial objects and the formation of subsequent fractal patterns which vary with the fractional operator (the derivative order). The results prove that we are in presence of differential systems capable of artificially structuring fractals using mathematical concepts, numerical techniques and simulations. Thus, the use of mathematical concepts to re-create features that usually occur in a natural way proves to be a prowess as related applications are many for applied scientists and engineers.

Keywords: Real life phenomena, rock fracture, wave motion, neuron sciences, differential models, three-dimensional fractal patterns; fractal-fractional modeling; numerical solution; exponential and Mittag-leffler laws.

1 Prelude

The Vice-Principal, Research, Postgraduate, Innovation and Commercialization, the Acting Vice Principal Teaching, Learning, Community Engagement and Student Support, The Executive Dean, College of Science, Engineering and Technology (CSET), Directors of Schools and Chairs of Departments here present, colleagues, students, friends, Family

members, ladies and gentlemen. It is indeed my honors and a huge privilege to present this inaugural lecture titled *Impacts of fractional and fractal differential operators in applied sciences* here in the University of South Africa, known as the biggest university in Africa.

When I decided to continue my studies to the PhD level after seven years of teaching high school mathematics in Canada, I was not really aware of the multiple challenges that will mark out my road during the journey. I had to fully rely on my supervisors and mentors to make my first steps into the world of research. Hence, after I graduated my PhD in the topic of mathematical modeling related to transport models, I wanted to continue my work in mathematical modeling, in order to generalize and improve my PhD research studies.

At that time, I had little knowledge on the calculus with derivative of fractional order and related fractal differential operators. The reason is simple: That is also the period where these differential operators were being developed and proposed for the first time. I then involved myself in various collaborations and discussions with imminent experts in the field to better seize the concepts. It appeared that fractal and fractional differential operators can solve number of outstanding issues found in applied sciences, but not all of them.

This motivated me to look at that particular direction and see how I can bring my little contribution to develop and improve the preceding results that exist in the domain. Hence, my journey began.

2 Differential operators in fractional calculus

2.1 Some preliminaries: Application in real life

In real life around us, we can start with a simple application of fractional calculus, that is the decomposition of a dead body mass as shown in Fig. 1. Such dynamic can be described by the relaxation function $g(t) = E_\gamma(-t^\gamma)$ as depicted in Fig. 2. It shows that as the value of the parameter γ decreases from 1 to 0, the relaxation function $E_\gamma(-t^\gamma)$ changes from the exponential decay function $g(t) = \mathrm{e}^{-t}$ (when $\gamma = 1$) to the hyperbolic decay function $g(t) = (1-t^\gamma)^{-1}$ (when $\gamma \sim 0$). Hence, when γ is smaller than 1, the initial fall of the curve is steep with faster rate and as the time increases, the fall happens with slower rate.

Another real life application are fractal type-patterns that exist all around us as shown in Fig. 3-Fig. 8. Another domain of interest is the rock fracture (Fig. 9-Fig. 10) that has become important in the fight against the global warming.

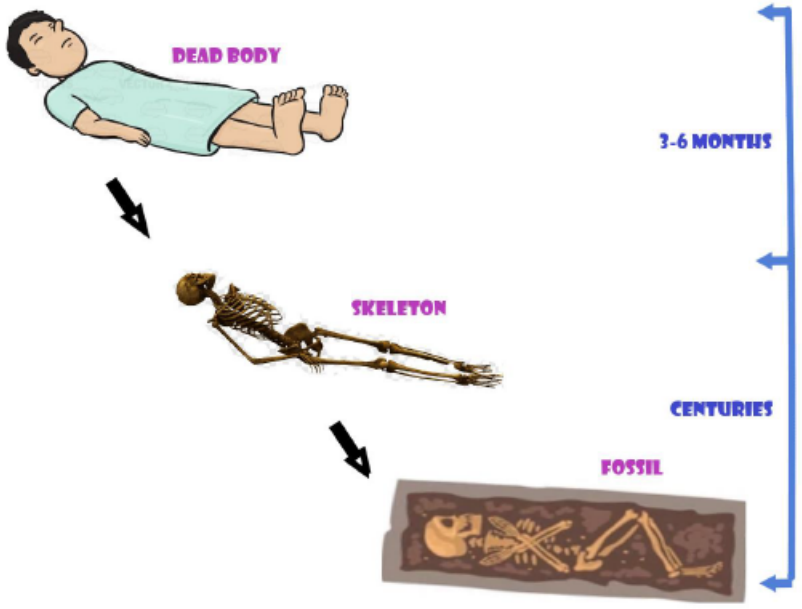

Fig. 1: Decomposition of a dead body mass.

2.2 Recent development in fractional calculus operators

At the beginning of 2015, two Italian researchers, Caputo and Fabrizio [1, (Caputo et al. 2015)] introduced a new fractional derivative with non-singular kernel (called the Caputo-Fabrizio derivative (CFD)). Recall that the field of mathematical modeling with derivative of fractional order, the old classical and most popular differential operators remain the Riemann–Liouville and the Caputo derivatives respectively defined as

$$D_t^{\gamma} u(t) = \frac{1}{\Gamma(1-\gamma)} \frac{d}{dt} \int_0^t (t-\tau)^{-\gamma} u(\tau)\, d\tau, \tag{1}$$

$0 < \gamma \leq 1$ and

$$D_t^{\gamma} u(t) = \frac{1}{\Gamma(1-\gamma)} \int_0^t (t-\tau)^{-\gamma} \frac{du}{d\tau}(\tau)\, d\tau, \tag{2}$$

$0 < \gamma \leq 1$. Then, the new version, that of the Caputo-Fabrizio is mathematically defined as

$${}^{c}D_t^{\gamma} u(t) = \frac{M(\gamma)}{(1-\gamma)} \int_0^t \frac{du}{d\tau}(\tau) \exp\left(-\frac{\gamma(t-\tau)}{1-\gamma}\right) d\tau, \tag{3}$$

and usually applied to a continuous function u and depends on the order of the differentiation γ and a normalisation function $M(\gamma)$ such that

$$M(0) = M(1) = 1 \tag{4}$$

Their initial motivation was to address open and unsolved issues still occurring in some applied science fields such as thermal media and electromagnetic. Another motivation

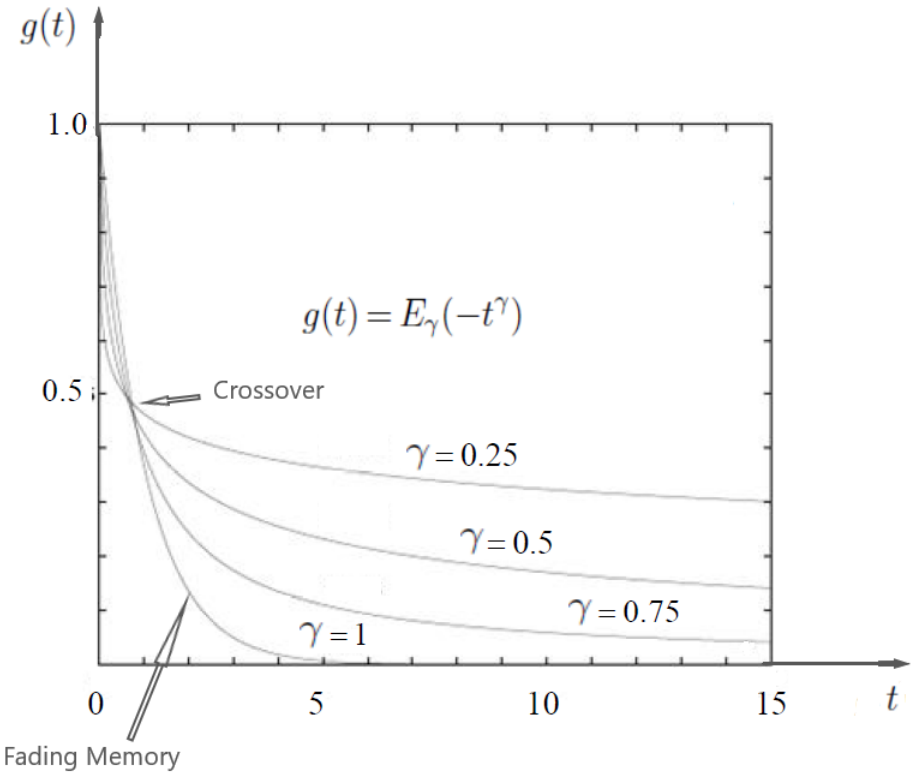

Fig. 2: Mittag-Leffler function E_γ as decay function for $\gamma \in [0,1]$. We observe in that figure the dynamics of relaxation function $g(t) = E_\gamma(-t^\gamma)$. It shows that as the value of the parameter γ decreases from 1 to 0, the relaxation function $E_\gamma(-t^\gamma)$ changes from the exponential decay function $g(t) = \mathrm{e}^{-t}$ (when $\gamma = 1$) to the hyperbolic decay function $g(t) = (1-t^\gamma)^{-1}$ (when $\gamma \sim 0$. It also shows that γ is smaller than 1, the initial fall of the curve is steep with faster rate and as the time increases, the fall happens with slower rate.

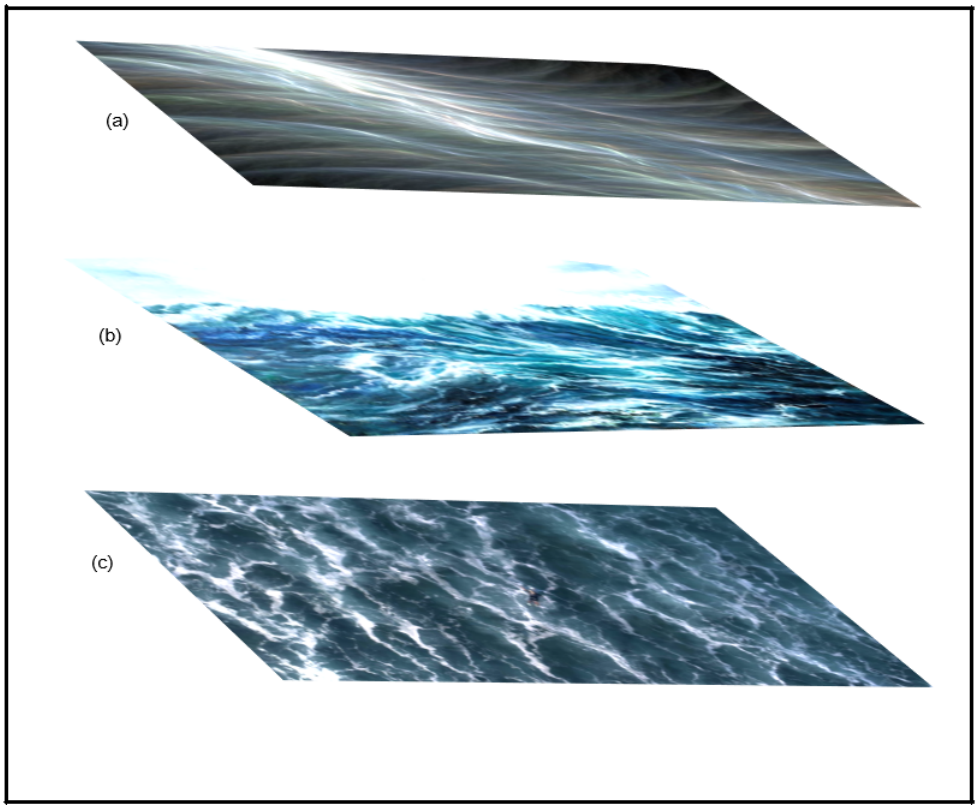

Fig. 3: Water or ocean waves involved in fractal type-patterns. The fractal motifs here are naturally formed due to the natural movements and shocks created by the wind on the water's (ocean's) surface.

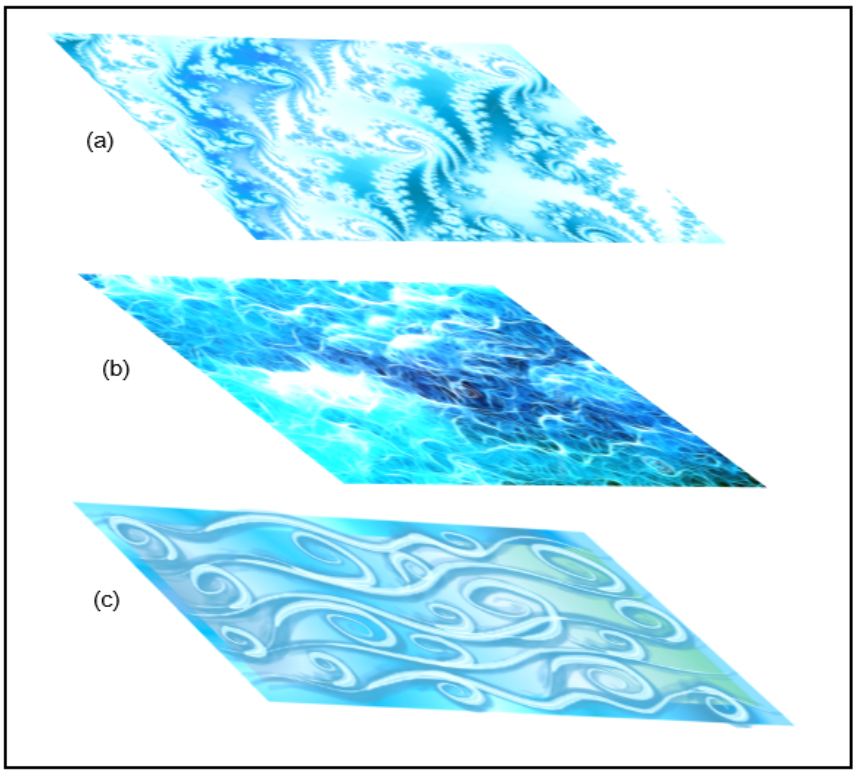

Fig. 4: Water or ocean waves involved in fractal type-motifs. The fractal patterns here are artificially (numerically) formed due to mathematical simulations issued from modeling the type of movements and shocks observed on the water's (ocean's) surface.

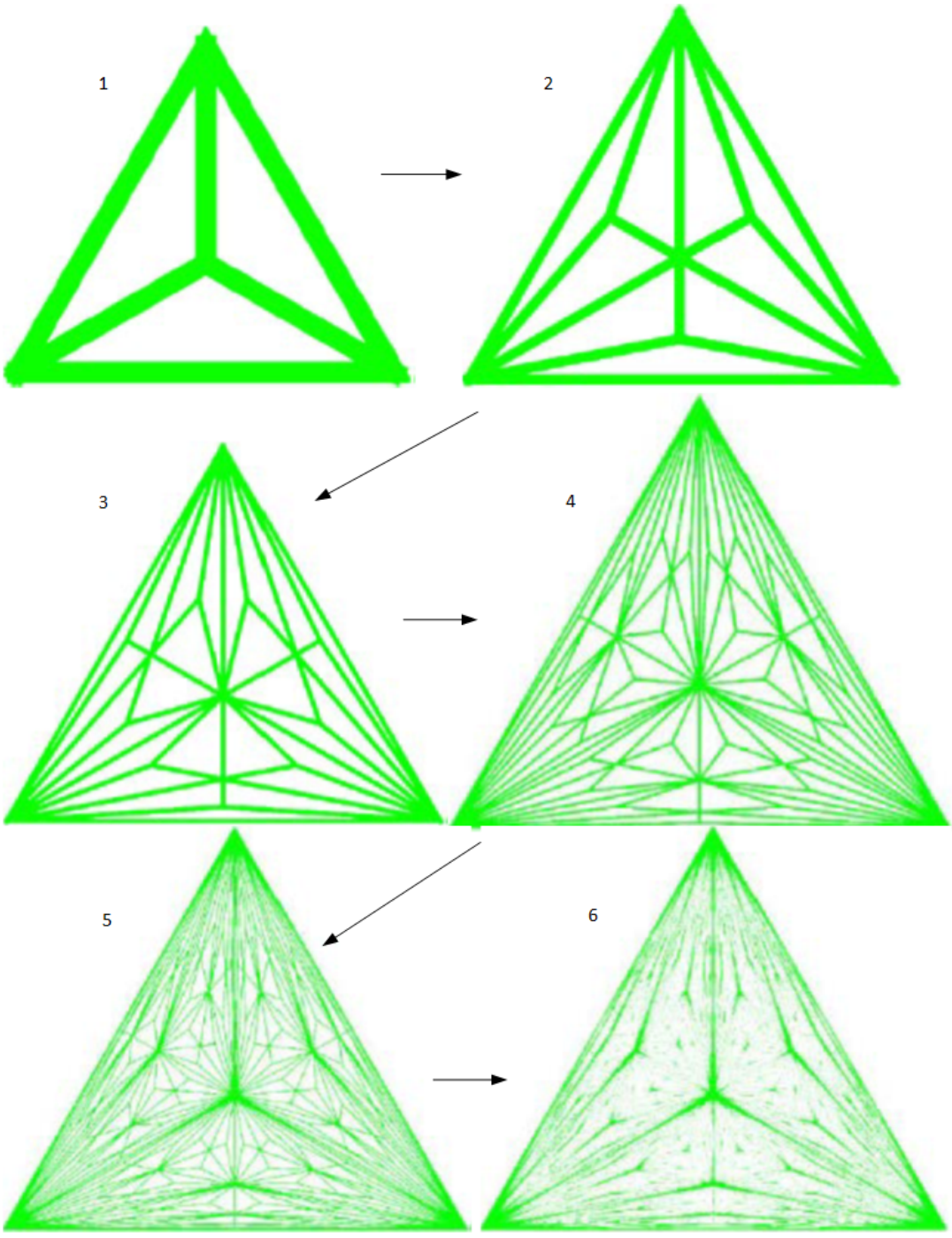

Fig. 5: A fractal structure with mathematical simulations. An initial equilateral triangle is divided into three identical and smaller ones via its apexes. The same procedure is repeated again and again for each of the smaller triangles to finally obtain the perfect fractal representation shown in step 6.

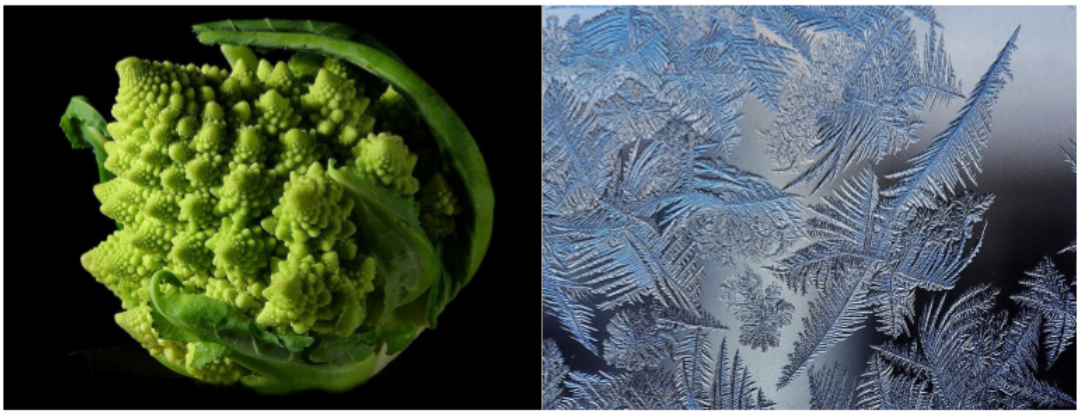

Fractal patterns in broccoli

Fractal patterns in Frost

Fig. 6: Fractal structure in nature.

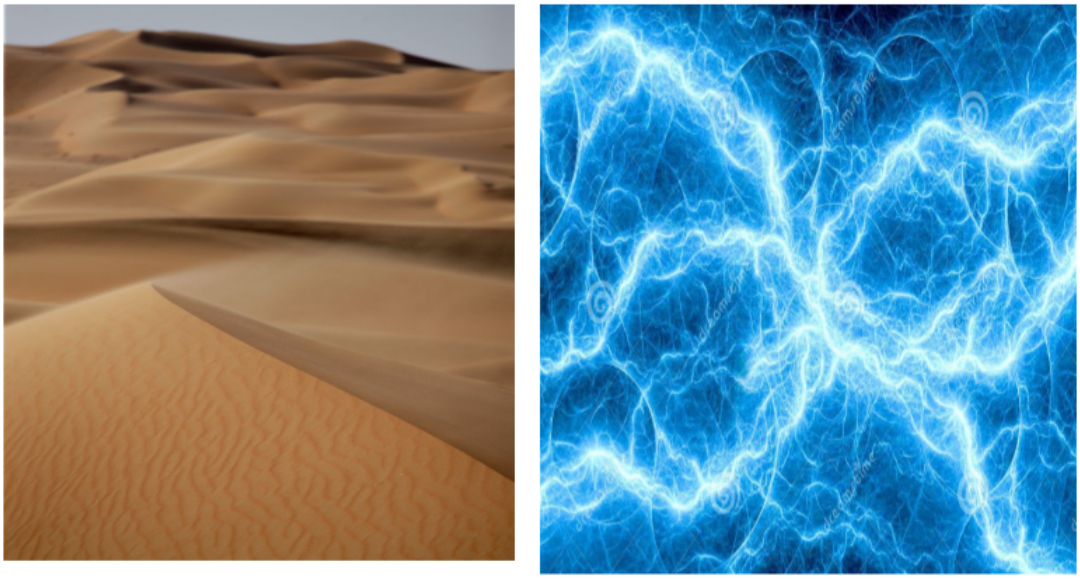

Fractal patterns in desert

Fractal patterns in lightning

Fig. 7: Fractal structure in nature

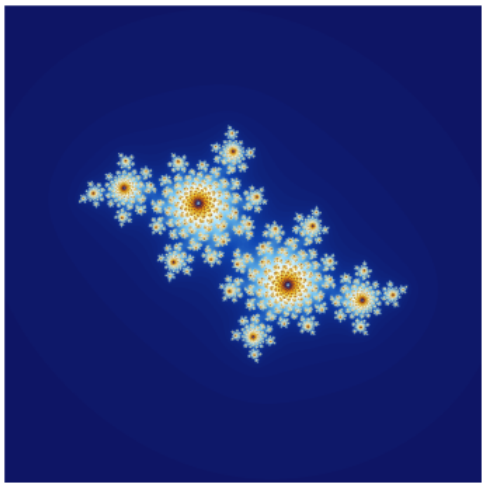

Fig. 8: Fractal structure in maths: Julia set $J(f_c) = \{z \in \mathbb{C} : |f_c^n(z)| \leq 2\}$, modelling $f_c(z) = z^2 + c$ with $c = (\varphi - 2) + (\varphi - 1)i = -0.4 + 0.6i$

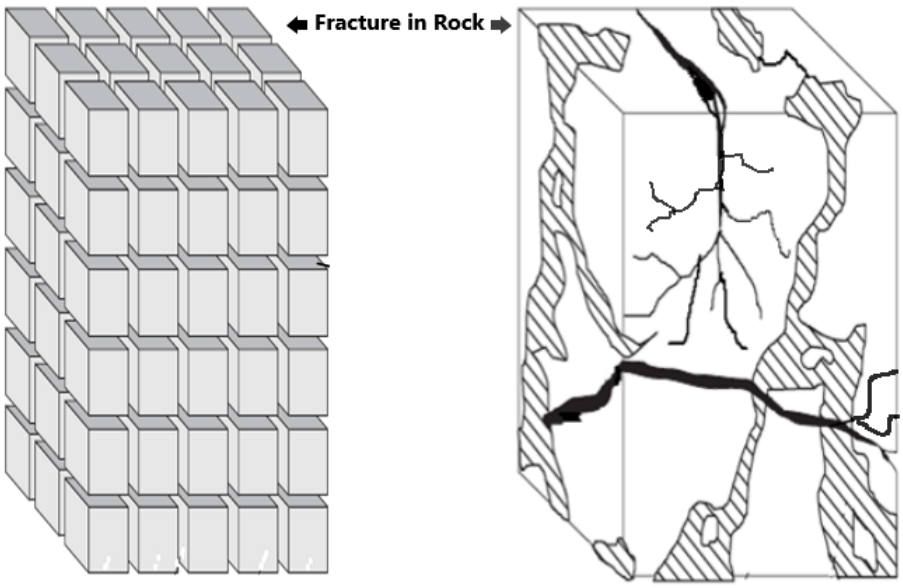

Fig. 9: Types of fissure processes in rock with the homogenized one (left) and the most common one (right)

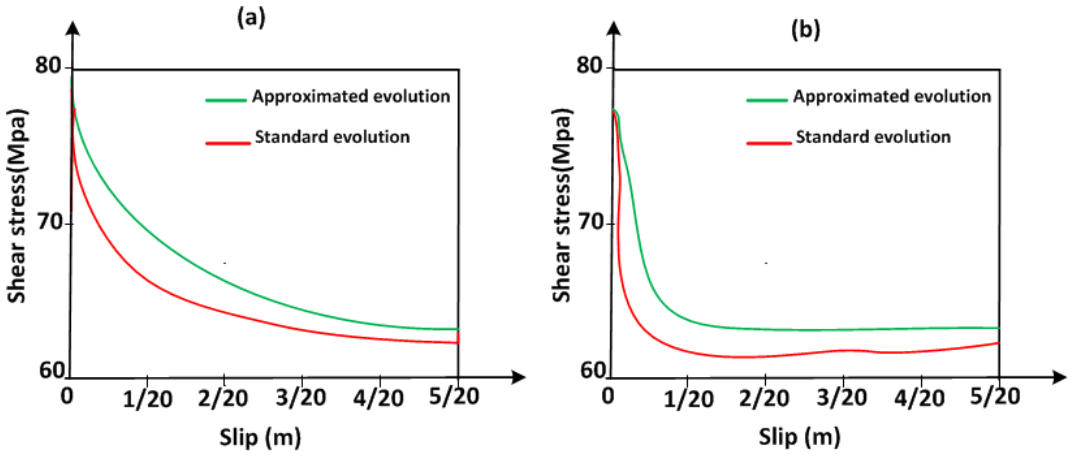

Fig. 10: Shear stress evolution of rock fissure process as function of slip for the homogenized one (a) and the most common one (b) corresponding to Fig. 9

for developing such a class of differential operators is their application to some real life processes with memory, including heat conduction in materials with memory, electrodynamics with memory or visco-elasticity. They have also proven to be suitable in approaching processes found in nonlinear conservation laws or in describing problems related to fatigue and usury. That 2015's initial paper, considered today as a pioneer paper, generated an equally innovative and important series of articles proposing other differential operators with no singular kernels widely used today in the field mathematical modeling. in fact, it started with

- Losada and Nieto [2, (Caputo et al. 2015)] who improved the definition of the CFD by proposition the following version.

$$ {}^{cf}D_t^{\gamma}u(t) = \frac{(2-\gamma)M(\gamma)}{2(1-\gamma)}\int_0^t \frac{du}{d\tau}(\tau)\exp\left(-\frac{\gamma(t-\tau)}{1-\gamma}\right)d\tau. \tag{5} $$

- Losada and Nieto proposed at the same time the fractional integral (anti-derivative) associated to the CFD as

$$ {}^{cf}I_t^{\gamma}u(t) = \frac{2(1-\gamma)}{(2-\gamma)M(\gamma)}u(t) + \frac{2\gamma}{(2-\gamma)M(\gamma)}\int_0^t u(\tau)\,d\tau, \tag{6} $$

  $\gamma \in [0,1]$ $t \geq 0$.

- Doungmo Goufo and Atangana [3, (Doungmo Goufo et. al 2016))] proposed the related Riemann-Liouville version of the CFD (also called New Riemann-Liouville derivative) defined for the order γ, $0 < \gamma \leq 0$ by

$$ {}^{NRL}D_t^{\gamma}u(t) = \frac{(2-\gamma)M(\gamma)}{2(1-\gamma)}\frac{d}{dt}\int_0^t u(\tau)\exp\left(-\frac{\gamma}{1-\gamma}(t-\tau)\right)d\tau \tag{7} $$

- More studies and questions in the same domain raised the issue of locality for that operator and then, Atangana and Beleanu [4, (Atangana et al. 2016)] modified the kernel of that operator and proposed the fractional derivative with non-singular and non-local kernel in Caputo sense and based on the one parameter Mittag-Leffler function,

$$E_\gamma(z)=\sum_{k=0}^{\infty}\frac{z^k}{\Gamma(\gamma k+1)},\quad \gamma\in\mathbb{C},\mathcal{R}(\gamma)>0 \tag{8}$$

  This operator is known today as the Atangana-Baleanu fractional derivative of order $\gamma,\ 0<\gamma\leq 0$ reading as

$${}^{ABC}D_t^\gamma u(t)=\frac{W(\gamma)}{(1-\gamma)}\int_0^t\frac{du}{d\tau}(\tau)\,E_\gamma\left[-\frac{\gamma(t-\tau)^\gamma}{1-\gamma}\right]d\tau,\quad 0<\gamma\leq 1 \tag{9}$$

  with the unknowns keeping the same meaning as in (3), except for w that belongs to the following Sobolev space of order one

$$H^1(a,e)=\{s:s,\frac{d}{dt}s\in L^2(a,e)\}. \tag{10}$$

- In the same momentum, Doungmo Goufo [5, (Doungmo Goufo 2016))] used the two-parameter Mittag-Leffler function to develop and proposed the Caputo-sense two-parameter fractional derivative with non-local and non-singular kernel of order γ knowing β, defined as

$${}^{GC}D_t^{\gamma,\beta}u(t)=\frac{\beta M(\gamma,\beta)}{(\beta-\gamma)}\int_0^t\dot{u}(\tau)\,(t-\tau)^{\beta-1}E_{\gamma,\beta}\left[-\frac{\gamma\beta(t-\tau)^\gamma}{\beta-\gamma}\right]d\tau, \tag{11}$$

  where $\beta\in\mathbb{R}$ and $M(\gamma,\beta)$ defines a two-variable normalization function such that $M(0,1)=M(1,1)=1$.

  Indeed, the same as the exponential function $f(z)=e^z$ is the solution of the ordinary differential equation

$$\frac{df(z)}{dz}=f(z),$$

  the one-parameter Mittag-Leffler function

$$E_\gamma(z)=\sum_{k=0}^{\infty}\frac{z^k}{\Gamma(\gamma k+1)},\quad \gamma\in\mathbb{C},\mathcal{R}(\gamma)>0 \tag{12}$$

  is the solution of the fractional differential equation (FDE)

$$\frac{d^\gamma f(z)}{dz^\gamma}=f(z).$$

Moreover, this function plays a significant role in the study of systems with fractional differential equations and is used to mathematically model several physical dynamics. For instance, it makes the connection between asymptotic approximation $\frac{z^{-\gamma}}{\Gamma(1-\gamma)} \sim E_\gamma(-z^{-\gamma})$ (inverse power law) for large argument z and stretched exponentials $\exp\left(-\frac{z^\gamma}{\Gamma(1+\gamma)}\right) \sim E_\gamma(-z^{-\gamma})$ for small argument z. This property is very important in investigation of relaxation process happening in general physics, disordered systems and fractional Brownian motion [6**? ?** –8]. A great development of the fractional calculus theory was made possible by the introduction of number of variants of Mittag-Leffler function since the early 1900s. One of them is the two-parameter Mittag-Leffler function

$$E_{\gamma,\beta}(z) = \sum_{k=0}^{\infty} \frac{z^k}{\Gamma(\gamma k+\beta)}, \quad \gamma,\beta,\ z\in\mathbb{C}, \mathcal{R}(\gamma)>0, \mathcal{R}(\beta)>0, \tag{13}$$

also called the generalized Mittag-Leffler function.

- The Riemann–Liouville sense of the two-parameter fractional derivative can be defined in a similar way as the later definition.

2.3 The Fractal with fractional operation

The fractal-fractional derivatives [9–11] have caught the attention of many researchers recently especially due to their capability to describe and address number of local or non-local phenomena found in the natural environment surrounding us. They are also able to respect and preserve the fractal structure of the phenomenon they study. There exist many definitions related to the different types of kernel used in fractal-fractional theory. We define some of then in the following lines.

Definition *2.1.* Let $\Omega \in \mathbb{R}^3, \quad T \in \mathbb{R}$. Suppose that $W(t,x) : (0,T)\times\Omega \to \mathbb{R}$ is fractal differentiable with respect to the variable $t \in (0,T)$.

1. We define the Riemann-Liouville sense fractal-fractional derivative ${}^{FRp}D_t^\gamma W$ of W with the power law kernel as

$${}^{FRp}D_t^\gamma W(t,x) = \frac{1}{\Gamma(1-\gamma)} \frac{\partial}{\partial t^\gamma} \int_0^t W(\varrho,x)\,(t-\varrho)^{-\gamma} d\varrho, \tag{14}$$

where $\frac{\partial}{\partial t^\gamma} W$ is defined as

$$\frac{\partial}{\partial t^\gamma} W(t,x_0) = \lim_{t\to t_0} \frac{W(t,x) - W(t,x_0)}{t^\gamma - t_0^\gamma}$$

with γ representing the derivative order.

Furthermore, we formulate its generalized definition as

$$^{FRp}D_t^{\gamma,\iota}W(t,x)=\frac{1}{\Gamma(1-\gamma)}\frac{\partial^\iota}{\partial t^\gamma}\int_0^t W(\varrho,x)(t-\varrho)^{-\gamma}d\varrho, \tag{15}$$

with $\iota>0$ and $\frac{\partial^\iota}{\partial t^\gamma}W$ given by

$$\frac{\partial^\iota}{\partial t^\gamma}W(t,x_0)=\lim_{t\to t_0}\frac{W^\iota(t,x)-W^\iota(t,x_0)}{t^\gamma-t_0^\gamma}.$$

2. We define the Caputo sense fractal-fractional derivative $^{FCp}D_t^\gamma W$ of W with power law kernel as

$$^{FCp}D_t^\gamma W(t,x)=\frac{1}{\Gamma(1-\gamma)}\int_0^t\frac{\partial}{\partial\varrho^\gamma}W(\varrho,x)(t-\varrho)^{-\gamma}d\varrho, \tag{16}$$

with γ representing the derivative order.

Furthermore, we formulate its generalized definition as

$$^{FCp}D_t^{\gamma,\iota}W(t,x)=\frac{1}{\Gamma(1-\gamma)}\int_0^t\frac{\partial^\iota}{\partial\varrho^\gamma}W(\varrho,x)(t-\varrho)^{-\gamma}d\varrho, \tag{17}$$

3. We define the Riemann-Liouville sense fractal-fractional derivative $^{FRe}D_t^\gamma W$ of W with the exponential kernel law as:

$$^{FRe}D_t^\gamma W(t,x)=\frac{\mathbf{r}(\gamma)}{(1-\gamma)}\frac{\partial}{\partial t^\gamma}\int_0^t W(\varrho,x)\exp\left(\frac{-\gamma(t-\varrho)}{1-\gamma}\right)d\varrho, \tag{18}$$

where $\mathbf{r}(0)=\mathbf{r}(1)=1$ with

its generalized definition is formulated as

$$^{FRe}D_t^{\gamma,\iota}W(t,x)=\frac{\mathbf{r}(\gamma)}{(1-\gamma)}\frac{\partial^\iota}{\partial t^\gamma}\int_0^t W(\varrho,x)\exp\left(\frac{-\gamma(t-\varrho)}{1-\gamma}\right)d\varrho. \tag{19}$$

We can associate to (18) its corresponding anti-derivative which is necessary for the analysis and solvability of the model. Then, the fractal-fractional integral of fractional order γ, is defined as follows:

$$^{FRe}I_t^\gamma g(t,\mathbf{y})=\frac{\gamma(1-\gamma)t^{\gamma-1}g(t,\mathbf{y})}{M(\gamma)}+\frac{\gamma^2}{M(\gamma)}\int_0^t\alpha^{\gamma-1}g(\alpha,\mathbf{y})d\alpha,\quad t>0. \tag{20}$$

4. We define the Caputo sense fractal-fractional derivative $^{FCe}D_t^\gamma W$ of W with the exponential kernel law as:

$$^{FCe}D_t^\gamma W(t,x)=\frac{\mathbf{r}(\gamma)}{(1-\gamma)}\int_0^t\frac{\partial}{\partial\varrho^\gamma}W(\varrho,x)\exp\left(\frac{-\gamma(t-\varrho)}{1-\gamma}\right)d\varrho, \tag{21}$$

with

its generalized definition is formulated as

$$^{FCe}D_t^{\gamma,\iota}W(t,x) = \frac{\mathbf{r}(\gamma)}{(1-\gamma)}\int_0^t \frac{\partial^\iota}{\partial\varrho^\gamma}W(\varrho,x)\exp\left(\frac{-\gamma(t-\varrho)}{1-\gamma}\right)d\varrho. \tag{22}$$

5. We define the Riemann-Liouville sense fractal-fractional derivative $^{FRm}D_t^\gamma W$ of W with the Mittag-Leffler kernel law as

$$^{FRm}D_t^\gamma W(t,x) = \frac{\mathbf{r}(\gamma)}{(1-\gamma)}\frac{\partial}{\partial t^\gamma}\int_0^t W(\varrho,x)\,E_\gamma\left(\frac{-\gamma(t-\varrho)^\gamma}{1-\gamma}\right)d\varrho, \tag{23}$$

with $\mathbf{r}(\gamma)$ representing a regularization function and γ representing the derivative order.

Its generalized definition is formulated as

$$^{FRm}D_t^{\gamma,\iota}W(t,x) = \frac{\mathbf{r}(\gamma)}{(1-\gamma)}\frac{\partial^\iota}{\partial t^\gamma}\int_0^t W(\varrho,x)\,E_\gamma\left(\frac{-\gamma(t-\varrho)^\gamma}{1-\gamma}\right)d\varrho. \tag{24}$$

6. We define the Caputo sense fractal-fractional derivative $^{FCm}D_t^\gamma W$ of W with the Mittag-Leffler kernel law as

$$^{FCm}D_t^\gamma W(t,x) = \frac{\mathbf{r}(\gamma)}{(1-\gamma)}\int_0^t \frac{\partial}{\partial\varrho^\gamma}W(\varrho,x)\,E_\gamma\left(\frac{-\gamma(t-\varrho)^\gamma}{1-\gamma}\right)d\varrho, \tag{25}$$

with $\mathbf{r}(\gamma)$ representing a regularization function and γ representing the derivative order.

Its generalized definition is formulated as

$$^{FCm}D_t^{\gamma,\iota}W(t,x) = \frac{\mathbf{r}(\gamma)}{(1-\gamma)}\int_0^t \frac{\partial^\iota}{\partial\varrho^\gamma}W(\varrho,x)\,E_\gamma\left(\frac{-\gamma(t-\varrho)^\gamma}{1-\gamma}\right)d\varrho. \tag{26}$$

Some of the definitions above refer to differential operators with no singular kernels (DONoSK) and have so far proven to have number of applications in applied sciences including applied mathematics, bio-mathematics, bio-physics, economics, mathematical epidemiology, mathematical ecology. Tools used here are dynamical systems, systems of differential equations, fractional differential equations, game dynamical systems with learning, fractional calculus, perturbation methods, linear nonlinear integro-differential equations, transport equation, (Aguilar Gomez 2017, Alkahtani 2016, Morales-Delgado, 2017, Doungmo Goufo 2017, Doungmo Goufo 2018, Doungmo Goufo 2019, Doungmo Goufo et al, 2018) . In particular, Doungmo Goufo (Doungmo Goufo 2016 and Doungmo Goufo et al. June 2018) proved that this derivative can also be applied to more additional areas including chaos theory, wave motion, atmospheric convection, relaxation and diffusion.

These differential operators with no singular kernels also leaded to the development of the Fourier transform of fractional gradient and fractional gradient divergence. Moreover the basic concepts under which lie the DONoSK are the convolution process and spatial filtering. This therefore represents the sources of the motivation for this research project which can be expressed as follows: There is a lot to do with the DONoSK deeply involving the Fourier transform, spatial filtering and convolution process which are three great concepts widely used in signal / image processing and its applications.

3 Applications of some differential operators with no singular kernels

3.1 Preliminaries on the model

Before processing with numerical simulations, we provide in this section existence and uniqueness results for the solution of the following 7th order KdV equation with a single perturbation level, expressed with the fractal fractional operator as

$$^{FRe}D_t^{\gamma} g(t,x) = -6gg_x - g_{xxx} + g_{xxxxx} - \kappa g_{xxxxxxx} \tag{27}$$

with the initial condition

$$g(0,x) = u(x), \tag{28}$$

where κ represents the perturbation parameter, $^{FRe}D_t^{\gamma}$ is the fractal-fractional derivative of fractional order γ of the function g in Riemann-Liouville sense combined with exponential law as defined in (18).

The standard classical version of this model with $\gamma = 1$ leading to $^{FRe}D_t^1 g(t) = g'(t)$, yields the system

$$\frac{\partial g(t,x)}{\partial t} = -6gg_x - g_{xxx} + g_{xxxxx} - \kappa g_{xxxxxxx}. \tag{29}$$

For this model, traveling waves in the form $g(x,t) = g(x+\psi t) = g(\varepsilon)$, can be investigated where ψ is the wave's speed. Performing the transformation into an ODE of the 7th order KdV equation (29), we set, $g_x = g_\varepsilon \cdot \varepsilon_x = g_\varepsilon$ and $g_t = g_\varepsilon \cdot \varepsilon_t = \psi g_\varepsilon$ and we obtain the following ODE

$$-\psi g_\varepsilon - 6ug_\varepsilon - g_{\varepsilon\varepsilon\varepsilon} + g_{\varepsilon\varepsilon\varepsilon\varepsilon\varepsilon} - \kappa g_{\varepsilon\varepsilon\varepsilon\varepsilon\varepsilon\varepsilon\varepsilon} = 0. \tag{30}$$

Integrating this model with respect ε gives

$$-\psi g - 3g^2 - g_{\varepsilon\varepsilon} + g_{\varepsilon\varepsilon\varepsilon\varepsilon} - \kappa g_{\varepsilon\varepsilon\varepsilon\varepsilon\varepsilon\varepsilon} = 0. \tag{31}$$

For the sake of simplicity, we consider that the wave vanishes at infinity, then

$$\lim_{\varepsilon\to\pm\infty} g(\varepsilon) = \lim_{\varepsilon\to\pm\infty} g_\varepsilon(\varepsilon) = \cdots = \lim_{\varepsilon\to\pm\infty} g_{\varepsilon\varepsilon\varepsilon\varepsilon\varepsilon\varepsilon\varepsilon}(\varepsilon) = 0 \tag{32}$$

Here we do not take into account the constant of integration with respect to ε that vanishes when boundary conditions (32) are considered. Without lost of generality, we neglect here the term $\kappa g_{\varepsilon\varepsilon\varepsilon\varepsilon\varepsilon\varepsilon}$ which expresses the higher order perturbation. Hence,

$$-\psi g - 3g^2 - g_{\varepsilon\varepsilon} + g_{\varepsilon\varepsilon\varepsilon\varepsilon} = 0. \tag{33}$$

The transformation of this equation into 4 different ODEs makes it possible to solve it numerically. Hence,

$$\begin{aligned} g_\varepsilon &= w \\ g_{\varepsilon\varepsilon} &= w_\varepsilon = y \\ g_{\varepsilon\varepsilon\varepsilon} &= y_\varepsilon = z \\ g_{\varepsilon\varepsilon\varepsilon\varepsilon} &= z_\varepsilon = \psi g + 3g^2 + y. \end{aligned} \tag{34}$$

Graphical representations are performed in the phase-space $(g, g_\varepsilon, g_{\varepsilon\varepsilon})$ as shown in Fig. 11 and Fig. 12. In fact, in Fig. 11 we can observe the graphical representation of the system (29) without higher order perturbation term in the phase-space $(g, g_\varepsilon, g_{\varepsilon\varepsilon})$ for $\gamma = 1$ (standard well known case). On top, it shows that the soliton represented using its homoclinic orbit lies on a curved surface. At the bottom, we have its projected representation on the plane (g, g_ε). In Fig. 12 we observe similar behavior for system (27) without higher order perturbation term in the same phase-space $(g, g_\varepsilon, g_{\varepsilon\varepsilon})$ for $\gamma = 0.9$ (Fractal-fractional case). On top, it shows that the soliton represented using its homoclinic orbit still lies on a curved surface, but is characterized by more distortions in its trajectory in comparision to the standard case (Fig. 11). At the bottom, we have similar representation projected on the plane (g, g_ε).

3.2 Existence and uniqueness results

To establish and prove the existence of solutions to the system (27)-(28), we apply the anti-derivative (20) on both sides. This leads to the following equality,

$$g(t,x) - g(0,x) = {}^{FRe} I_t^\gamma \left(-6gg_x - g_{xxx} + g_{xxxxx} - \kappa g_{xxxxxxx}\right),$$

which also takes the form

$$\begin{aligned} g(t,x) - g(0,x) = {} & \frac{\gamma(1-\gamma)t^{\gamma-1}}{M(\gamma)} \left[-6gg_x(t,\mathbf{y}) - g_{xxx}(t,\mathbf{y}) + g_{xxxxx}(t,\mathbf{y}) - \kappa g_{xxxxxxx}(t,\mathbf{y})\right] \\ & + \frac{\gamma^2}{M(\gamma)} \int_0^t \alpha^{\gamma-1} \left[-6gg_x(\alpha,\mathbf{y}) - g_{xxx}(\alpha,\mathbf{y}) + g_{xxxxx}(\alpha,\mathbf{y}) - \kappa g_{xxxxxxx}(\alpha,\mathbf{y})\right] d\alpha. \end{aligned} \tag{35}$$

Let

$$\mathcal{W}(t,x,g,\kappa) = -6gg_x - g_{xxx}(t,x) + g_{xxxxx}(t,x) - \kappa g_{xxxxxxx}(t,x). \tag{36}$$

The analysis continues by looking for a real number $K \geq 0$ satisfying

$$\|\mathcal{W}(t,x,g,\kappa) - \mathcal{W}(t,x,f,\kappa)\| \leq K\|g - f\|$$

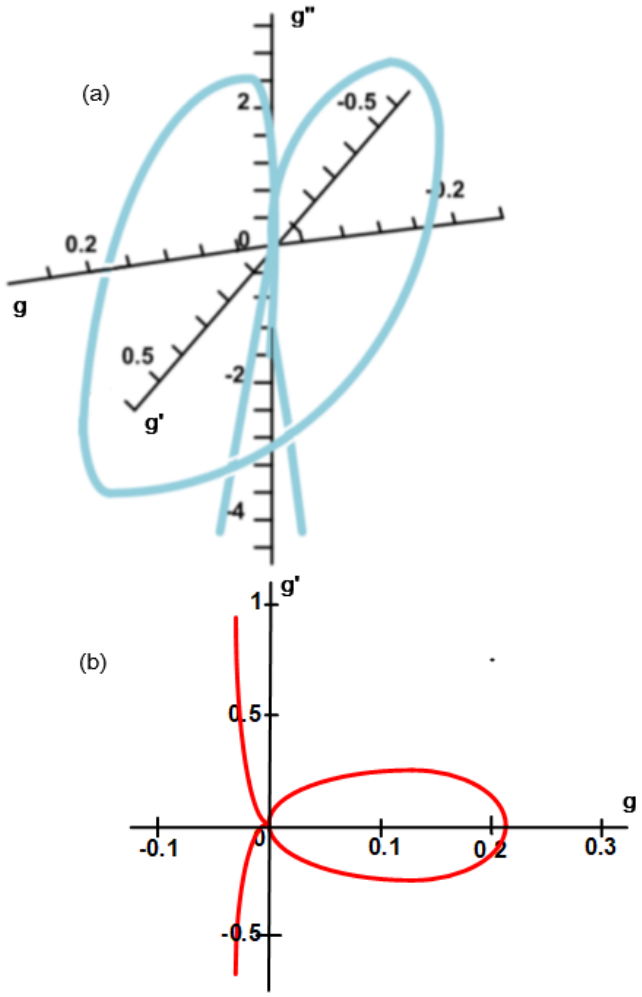

Fig. 11: Graphical representation of the system (29) without higher order perturbation term in the phase-space $(g, g_\varepsilon, g_{\varepsilon\varepsilon})$ for $\gamma = 1$ (standard well known case). On top, it shows that the soliton represented using its homoclinic orbit lies on a curved surface. At the bottom, we have its projected representation on the plane (g, g_ε).

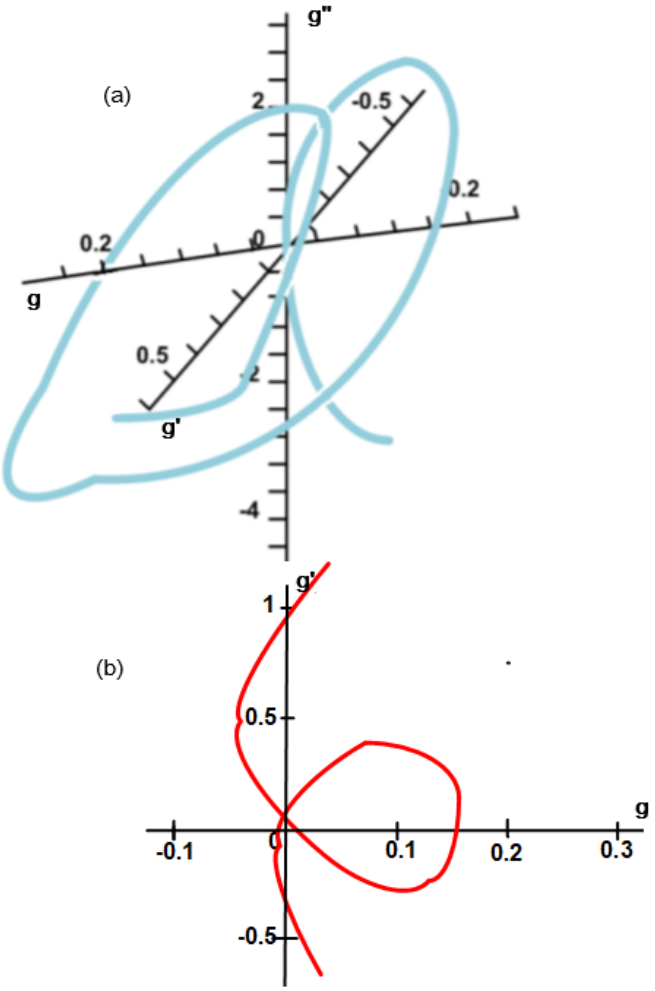

Fig. 12: Graphical representation of the system (29) without higher order perturbation term in the phase-space $(g, g_\varepsilon, g_{\varepsilon\varepsilon})$ for $\gamma = 0.9$ (Fractal-fractional case). On top, it shows that the soliton represented using its homoclinic orbit lies on a curved surface, but is characterized by more distortions in its trajectory in comparision to the standard case (Fig. 11). At the bottom, we have similar representation projected on the plane (g, g_ε).

Whence,

$$\begin{aligned}
&\mathcal{W}(t,x,g,\kappa)-\mathcal{W}(t,x,f,\kappa)\\
=&(-6gg_x(t,x)-g_{xxx}(t,x)+g_{xxxxx}(t,x)-\kappa g_{xxxxxxx}(t,x))\\
&-(-6ff_x(t,x)-f_{xxx}(t,x)+f_{xxxxx}(t,x)-\kappa f_{xxxxxxx}(t,x))\\
=&6(ff_x(t,x)-gg_x(t,x))+(f_{xxx}(t,x)-g_{xxx}(t,x))+(g_{xxxxx}(t,x)-f_{xxxxx}(t,x))\\
&+\kappa(f_{xxxxxxx}(t,x)-g_{xxxxxxx}(t,x)).
\end{aligned}$$

We make use of the standard properties of norm to have

$$\begin{aligned}
&\|\mathcal{W}(t,x,g,\kappa)-\mathcal{W}(t,x,f,\kappa)\|\\
&=\|6(ff_x-gg_x)+(f_{xxx}-g_{xxx})+(g_{xxxxx}-f_{xxxxx})+\kappa(f_{xxxxxxx}-g_{xxxxxxx})\|\\
&\leq 6\|ff_x-gg_x\|+\|f_{xxx}-g_{xxx}\|+\|g_{xxxxx}-f_{xxxxx}\|+\kappa\|f_{xxxxxxx}-g_{xxxxxxx}\|\\
&\leq 6\|\partial_x(f^2-g^)\|+\|\partial_{xxx}(f-g)\|+\|\partial_{xxxxx}(g-f)\|+\kappa\|\partial_{xxxxxxx}(f-g)\|.
\end{aligned}$$

Due to the fact that both functions g and f are assumed to be bounded, therefore there are two real constants $a_1>0$ and $a_2>0$ satisfying

$$\|g\|\leq a_1 \qquad \text{and} \qquad \|f\|\leq a_2. \tag{37}$$

Let now $a=\max(a_1,a_2)$, hence,

$$\|g\|\leq a \qquad \text{and} \qquad \|f\|\leq a. \tag{38}$$

At this stage, we can use the fact that the partial derivatives $\partial_x g$ and $\partial_x f$ verify the Lipschitz condition and therefore, there is a real number $R_1\geq 0$ satisfying

$$\begin{aligned}
&\|\mathcal{W}(t,x,g,\kappa)-\mathcal{W}(t,x,f,\kappa)\|\leq 6R_1\|f^2-g^\|+R_1^3\|f-g\|+R_1^5\|g-f\|+\kappa R_1^7\|f-g\|\\
&\leq 6R_1\|g+f\|\cdot\|g-f\|+R_1^3\|f-g\|+R_1^5\|g-f\|+\kappa R_1^7\|f-g\|\\
&\leq \left[12aR_1+R_1^3+R_1^5+\kappa R_1^7\right]\|g-f\|,
\end{aligned} \tag{39}$$

where we have used the bounded condition (28). Whence,

$$\|\mathcal{W}(t,x,g,\kappa)-\mathcal{W}(t,x,f,\kappa)\|\leq K\|g-f\|$$

with

$$K=12aR_1+R_1^3+R_1^5+\kappa R_1^7. \tag{40}$$

This completes the proof related to the Lipschitz property for the operator $\mathcal{W}$. The later proof makes it possible to state the following result:

Proposition 3.1. Assuming that the relation $\gamma(1-\gamma)t^{\gamma-1}K+K\gamma^2 t<M(\gamma)$ is satisfied, hence, there exists a unique solution to the 7th order KdV equation with a single perturbation level and expressed with the fractal fractional operator as given in (27)-(28):

$$\begin{cases} {}^{FRe}D_t^\gamma g(t,x)=-6gg_x-g_{xxx}+g_{xxxxx}-\kappa g_{xxxxxxx}\\ g(0,x)=u(x), \end{cases} \tag{41}$$

Proof. We start by referring to the system (35) which we rewrite as

$$g(t,x)-g(0,x)=\frac{\gamma(1-\gamma)t^{\gamma-1}}{M(\gamma)}\mathcal{W}(t,x,g,\kappa)+\frac{\gamma^2}{M(\gamma)}\int_0^t\alpha^{\gamma-1}\mathcal{W}(\alpha,x,g,\kappa)d\alpha \tag{42}$$

and that leads to the following iterative relation:

$$\begin{aligned} g_0(t,x)&=g(0,x)\\ g_n(t,x)&=\frac{\gamma(1-\gamma)t^{\gamma-1}}{M(\gamma)}\mathcal{W}(t,x,g_{n-1},\kappa)+\frac{\gamma^2}{M(\gamma)}\int_0^t\alpha^{\gamma-1}\mathcal{W}(\alpha,x,g_{n-1},\kappa)d\alpha. \end{aligned} \tag{43}$$

Now set

$$\underline{g}(t,x)=\lim_{n\to\infty}g_n(t,x), \tag{44}$$

Now we proceed by proving that the solution $\underline{g}(t,x)=g(t,x)$ is continuous. In fact, if we consider

$$U_n(t,x)=g_n(t,x)-g_{n-1}(t,x) \tag{45}$$

then, we can directly see that

$$g_n(t,x)=\sum_{p=0}^{n}U_p(t,x).$$

More explicitly,

$$\begin{aligned} U_n(t,x)&=\frac{\gamma(1-\gamma)t^{\gamma-1}}{M(\gamma)}\left[\mathcal{W}(t,x,g_{n-1},\kappa)-\mathcal{W}(t,x,g_{n-2},\kappa)\right]\\ &+\frac{\gamma^2}{M(\gamma)}\int_0^t\alpha^{\gamma-1}\left(\mathcal{W}(\alpha,x,g_{n-1},\kappa)-\mathcal{W}(\alpha,x,g_{n-2},\kappa)\right)d\alpha. \end{aligned} \tag{46}$$

Applying the norm property to this equation gives

$$\begin{aligned} \|U_n(t,x)\|&=\|g_n(t,x)-g_{n-1}(t,x)\|\\ &\leq\frac{\gamma(1-\gamma)t^{\gamma-1}}{M(\gamma)}\|\mathcal{W}(t,x,g_{n-1},\kappa)-\mathcal{W}(t,x,g_{n-2},\kappa)\|\\ &\quad+\frac{\gamma^2}{M(\gamma)}\left\|\int_0^t\alpha^{\gamma-1}\left[\mathcal{W}(\alpha,x,g_{n-1},\kappa)-\mathcal{W}(\alpha,x,g_{n-2},\kappa)\right]d\alpha\right\|\\ &\leq\frac{\gamma(1-\gamma)t^{\gamma-1}}{M(\gamma)}\|\mathcal{W}(t,x,g_{n-1},\kappa)-\mathcal{W}(t,x,g_{n-2},\kappa)\|\\ &\quad+\frac{\gamma^2}{M(\gamma)}\int_0^t\alpha^{\gamma-1}\|\mathcal{W}(\alpha,x,g_{n-1},\kappa)-\mathcal{W}(\alpha,x,g_{n-2},\kappa)\|d\alpha \end{aligned} \tag{47}$$

Application of Lipschitz constraint to $\mathcal{W}$ yields

$$\|U_n(t,x)\|\leq\frac{\gamma(1-\gamma)t^{\gamma-1}}{M(\gamma)}K\|g_{n-1}-g_{n-2}\|+\frac{K\gamma^2}{M(\gamma)}\int_0^t\alpha^{\gamma-1}\|g_{n-1}-g_{n-2}\|d\alpha$$

which can take the form

$$\|U_n(t,x)\| \leq \frac{\gamma(1-\gamma)t^{\gamma-1}}{M(\gamma)}K\|U_{n-1}\| + \frac{K\gamma^2}{M(\gamma)}\int_0^t \alpha^{\gamma-1}\|U_{n-1}\|d\alpha. \tag{48}$$

Integration followed by the use of standard properties of the iteration method from the system (48) give

$$\|U_n(t,x)\| \leq \left[\left(\frac{\gamma(1-\gamma)t^{\gamma-1}}{M(\gamma)}K\right)^n + \left(\frac{K\gamma^2 t}{M(\gamma)}\right)^n\right]u(x),$$

with $u(x) = g(0,x)$. Hence, we have explicitly proven that the solution to the model exists and is continuous.

Next, we have to show that the function

$$g(t,x) = \lim_{n\to\infty} g_n(t,x)$$

is the solution to the system (41). Whence, set

$$Q_n(t,x) = \underline{g}(t,x) - g_n(t,x) \qquad \text{with} \qquad n \in \mathbb{N}.$$

Taking (44), we should get $\lim_{n\to\infty} Q_n = 0$. This can be interpreted by saying that the existing gap between $\underline{g}(t,x)$ and $g_n(t,x)$ is vanishing when $n \to \infty$. Consider

$$\begin{aligned}\underline{g} - g_{n-1} &= \frac{\gamma(1-\gamma)t^{\gamma-1}}{M(\gamma)}\left[\mathcal{W}(t,x,g,\kappa) - \mathcal{W}(t,x,g_n,\kappa)\right] \\ &+ \frac{\gamma^2}{M(\gamma)}\int_0^t \alpha^{\gamma-1}\left(\mathcal{W}(\alpha,x,g,\kappa) - \mathcal{W}(\alpha,x,g_n,\kappa)\right)d\alpha,\end{aligned}$$

giving

$$\begin{aligned}\|\underline{g}(t,x) - g_{n+1}\| &\leq \frac{\gamma(1-\gamma)t^{\gamma-1}}{M(\gamma)}\|\mathcal{W}(t,x,g,\kappa) - \mathcal{W}(t,x,g_n,\kappa)\| \\ &+ \frac{\gamma^2}{M(\gamma)}\int_0^t \alpha^{\gamma-1}\|(\mathcal{W}(\alpha,x,g,\kappa) - \mathcal{W}(\alpha,x,g_n,\kappa)\|d\alpha \\ &\leq \frac{\gamma(1-\gamma)t^{\gamma-1}}{M(\gamma)}K\|g - g_n\| + \frac{K\gamma^2}{M(\gamma)}\int_0^t \alpha^{\gamma-1}\|g - g_n\|d\alpha \\ &\leq \frac{\gamma(1-\gamma)t^{\gamma-1}}{M(\gamma)}K\|Q_n\| + \frac{K\gamma^2}{M(\gamma)}\int_0^t \alpha^{\gamma-1}\|Q_n\|d\alpha\end{aligned} \tag{49}$$

Hence, $\lim_{n\to\infty} Q_n = 0$ and from the right-hand-side,

$$\lim_{n\to\infty} g_n = \underline{g}.$$

Just consider $g(t,x)=\underline{g}(t,x)$ as the continuous solution to the system (41). Moreover, making use of the Lipschitz condition of $\mathcal{W}$ we get

$$\begin{aligned}
&g(t,x)-\frac{\gamma(1-\gamma)t^{\gamma-1}}{M(\gamma)}\mathcal{W}(t,x,g,\kappa)-\frac{\gamma^2}{M(\gamma)}\int_0^t\alpha^{\gamma-1}\mathcal{W}(\alpha,x,g,\kappa)d\alpha\\
&=U_n(t,x)+\frac{\gamma(1-\gamma)t^{\gamma-1}}{M(\gamma)}\left(\mathcal{W}(\alpha,x,g_{n-1},\kappa)-\mathcal{W}(t,x,g,\kappa)\right)\\
&+\frac{\gamma^2}{M(\gamma)}\int_0^t\alpha^{\gamma-1}\left(\mathcal{W}(\alpha,x,g_{n-1},\kappa)-\mathcal{W}(t,x,g,\kappa)\right)d\alpha.
\end{aligned}\tag{50}$$

This yields

$$\begin{aligned}
&\left\|g(t,x)-\frac{\gamma(1-\gamma)t^{\gamma-1}}{M(\gamma)}\mathcal{W}(t,x,g,\kappa)-\frac{\gamma^2}{M(\gamma)}\int_0^t\alpha^{\gamma-1}\mathcal{W}(\alpha,x,g,\kappa)d\alpha\right\|\\
&=\|U_n(t,x)\|+\left(\frac{\gamma(1-\gamma)t^{\gamma-1}}{M(\gamma)}+\frac{\gamma^2}{M(\gamma)}\right)\|U_{n-1}(t,x)\|.
\end{aligned}\tag{51}$$

Applying both the initial condition and the limit as $n\to 0$ leads to

$$g(t,x)=u(x)+\frac{\gamma(1-\gamma)t^{\gamma-1}}{M(\gamma)}\mathcal{W}(t,x,g,\kappa)+\frac{\gamma^2}{M(\gamma)}\int_0^t\alpha^{\gamma-1}\mathcal{W}(\alpha,x,g,\kappa)d\alpha.$$

Uniqueness

Uniqueness result for the model can be proven by considering two separate functions g and f that verify the model (41) then, showing that g and f coincide.

$$\|g-f\|\leq\frac{\gamma(1-\gamma)t^{\gamma-1}}{M(\gamma)}K\|g-f\|+\frac{K\gamma^2t}{M(\gamma)}\|g-f\|,\tag{52}$$

equivalently

$$\|g-f\|\left(1-\frac{\gamma(1-\gamma)t^{\gamma-1}}{M(\gamma)}K-\frac{K\gamma^2t}{M(\gamma)}\right)\leq 0.$$

This proves that $g=f$ if

$$1>\frac{\gamma(1-\gamma)t^{\gamma-1}}{M(\gamma)}K-\frac{K\gamma^2t}{M(\gamma)}$$

where the Lipschitz condition for $\mathcal{W}$ has been applied. Thus, the proof of existence and uniqueness results for the 7th order KdV equation with a single perturbation level and expressed with the fractal fractional operator is complete. □

4 Some shapes of fractal traveling waves via numerical approximations

Sometimes waves traveling in a given direction do not behave as planned and this creates unusual shapes for the waves. To asses it, we consider the system

$${}^{FRe}D_t^{\gamma}g(t,x)=-6gg_x-g_{xxx}+g_{xxxxx}-\kappa g_{xxxxxxx}\tag{53}$$

to which the following localized initial condition is associated

$$g(0,x)=\sqrt{\frac{17\eta}{\nu}}\tanh^2\left(\sqrt{\frac{x}{\nu}}\right). \tag{54}$$

Recall that in the previous section, we have shown that solution to this type of non-linear system exists and is unique. However, finding and explicitly expressing its exact or approximated solution remain a challenging task. Other and easier ways would have been to apply some analytical methods such as integral transform or separation of variables methods. Using specialized function technique like that of Green function is also appropriate here but almost impossible to achieve. Therefore we can make use of one of few alternative methods relevant to this non-linear model: a semi-analytical approach. In this case, we consider the Laplace iterative technique to obtain a special solution that satisfy the non-linear system (53)–(54). To achieve it we start by considering the fractal-Laplace transform $\mathbb{L}$ and applying it on both sides of the model (53), which leads to

$$\frac{\gamma+(1-\gamma)s}{sM(\gamma)}\tilde{g}(s,x)-g(0,x)=\mathbb{L}(s,\ -6gg_x-g_{xxx}+g_{xxxxx}-\kappa g_{xxxxxxx}) \tag{55}$$

$$\tilde{g}(s,x)=\frac{sM(\gamma)}{\gamma+(1-\gamma)s}g(0,x)+\frac{sM(\gamma)}{\gamma+(1-\gamma)s}\mathbb{L}(s,\ -6gg_x-g_{xxx}+g_{xxxxx}-\kappa g_{xxxxxxx}).$$

Applying the inverse fractal-Laplace transform $\mathbb{L}^{-1}$ on both sides now gives

$$g(t,x)=M(\gamma)g(0,x)\mathbb{L}^{-1}(t,\ \frac{s}{\gamma+(1-\gamma)s})$$

$$+\mathbb{L}^{-1}\left(t,\ \frac{sM(\gamma)}{\gamma+(1-\gamma)s}\mathbb{L}(s,\ -6gg_x-g_{xxx}+g_{xxxxx}-\kappa g_{xxxxxxx})\right).$$

At this stage it is significant to make use of a special and generalized function. A function that returns its own expression when it is fractionally differentiated and integrated or simply differintegrated by any order. In the classical integer order calculus, such functions include are exponential and trigonometric functions while in fractional calculus, we have Mittag-Leffler functions and its variants such as the generalized R function. Then, using the generalized R function $R_{r,i}(\beta,t)$ [9, 12, 13] defined as

$$\mathbb{L}^{-1}\left(t,\frac{s^i}{s^r-\beta}\right)=\sum_{p=0}^{+\infty}\frac{\beta^p\ t^{(p+1)r-1-i}}{\Gamma((p+1)r-i)}=R_{r,i}(\beta,t)$$

leads to the following iteration scheme

$$\begin{aligned}
g_{n+1}(t,x)&=\beta(t,\gamma)g_n(t,x)\\
&\quad+\mathbb{L}^{-1}\left(t,\ \frac{sM(\gamma)}{\gamma+(1-\gamma)s}\mathbb{L}(s,\ -6g_n(g_n)_x-(g_n)_{xxx}+(g_n)_{xxxxx}-\kappa(g_n)_{xxxxxxx})\right)\\
g_0(t,x)&=g(0,x),
\end{aligned} \tag{56}$$

where

$$\beta(t,\gamma)=M(\gamma)\left[\sum_{p=0}^{+\infty}\frac{\left(\frac{\gamma}{\gamma-1}\right)^{p}\ t^{p-1}}{\Gamma(p)}\right].$$

Certainly leading to the solution $g(t,x)=\lim_{n\to\infty}g_n(t,x)$. Now following guidelines can be used to perform numerical approximations and simulations:

- $g_0(t,x)=g(0,x)$ is considered as initial input:

  Select j to be the number of terms in the computation process

  Denote by g_{app} the approximate solution.

  Let $g_{app}=g(0,x)=\sqrt{\frac{17\eta}{\nu}}\tanh^2\left(\sqrt{\frac{x}{\nu}}\right)$ and $g_{app}=g_{app}$.

- make use of : $g_{n+1}(t,x)=M(\gamma)\left[\sum_{p=0}^{+\infty}\frac{\left(\frac{\gamma}{\gamma-1}\right)^{p}\ t^{p-1}}{\Gamma(p)}\right]g_n(t,x)$ for the following terms

$$+\mathbb{L}^{-1}\left(\frac{sM(\gamma)}{\gamma+(1-\gamma)s}\mathbb{L}\left(-6g_n(g_n)_x-(g_n)_{xxx}+(g_n)_{xxxxx}-\kappa(g_n)_{xxxxxxx},s\right),t\right)$$

  Compute $X_n(t,x)=X_{n-1}(t,x)+g_{app}$

  Lastly we obtain $g_{app}(t,x)=X_n(t,x)+g_{app}$,

where

$$X_n(t,x)=\mathbb{L}^{-1}\left(\frac{sM(\gamma)}{\gamma+(1-\gamma)s}\mathbb{L}\left(-6g_n(g_n)_x-(g_n)_{xxx}+(g_n)_{xxxxx}-\kappa(g_n)_{xxxxxxx},s\right),t\right).$$

We also have Table 1 and Table 2 summarizing absolute errors done when performing numerical approximations. Note that those two tables show results from numerical approximations together with the corresponding absolute errors and coming from the schemes (57) and (58) representing the fractional cases ($\gamma=0.9$) and ($\gamma=0.7$)) respectively. It is

possible to make use of $\beta(s,\gamma)$, in order to get following results.

$$g(0,x) = \sqrt{\frac{17\eta}{\nu}}\tanh^2\left(\sqrt{\frac{x}{\nu}}\right)$$

$$\begin{aligned}
g_1(t,x) = {} & \beta(t,\ 0.9)g(0,x) + \frac{(1.700\times10^{-3})t\sqrt{d}}{k^{3/2}}\left\{1.233\frac{\sqrt{d}}{k^{1/2}} - \frac{3.467}{k^2} - \frac{273}{k^4} - \frac{78733\kappa}{k^6}\right. \\
& + \left(-\frac{2.237}{k^2} - \frac{133.200}{k^4} + \frac{77631\kappa}{k^6}\right)\coth\left(2\sqrt{\frac{x}{\nu}}\right) \\
& + \left(-\frac{0.102}{k^2} + \frac{173.700}{k^4} + \frac{14681\kappa}{k^6}\right)\coth\left(4\sqrt{\frac{x}{\nu}}\right) \\
& \left. + \left(\frac{0.372}{k^2} - \frac{13.730}{k^4} + \frac{476\kappa}{k^6}\right)\coth\left(6\sqrt{\frac{x}{\nu}}\right)\right\}\tanh^{12}\left(\sqrt{\frac{x}{\nu}}\right)\tanh\left(\sqrt{\frac{x}{\nu}}\right) \\
& + \frac{(1-\gamma)\Gamma(\gamma)t^{\gamma-1}\sqrt{d}}{k}\left\{0.223\frac{\sqrt{d}}{k} - \frac{3.830}{k^{1/4}} - \frac{332.303\kappa}{k^{1/6}}\right. \\
& + \left(-\frac{0.037}{k^{1/2}} - \frac{3.320}{k^{1/4}} + \frac{683\kappa}{k^{1/6}}\right)\coth\left(2\sqrt{\frac{x}{\nu}}\right) \\
& + \left(-\frac{0.030}{k^{1/2}} + \frac{3.820}{k^{1/4}} + \frac{641\kappa}{k^{1/6}}\right)\coth\left(4\sqrt{\frac{x}{\nu}}\right) \\
& \left. + \left(\frac{0.072}{k^{1/2}} - \frac{0.770}{k^{1/4}} + \frac{7.630\kappa}{k^{1/6}}\right)\coth\left(6\sqrt{\frac{x}{\nu}}\right)\right\}\frac{\tanh^6\left(\sqrt{\frac{x}{\nu}}\right)\tanh\left(\sqrt{\frac{x}{\nu}}\right)}{2^\gamma - \gamma}
\end{aligned} \tag{57}$$

$$\begin{aligned}
g_2(t,x) = {} & g_1(0,x) + \cdots \\
& \vdots
\end{aligned}$$

and

$$g(0,x) = \sqrt{\frac{17\eta}{\nu}}\tanh^2\left(\sqrt{\frac{x}{\nu}}\right)$$

$$\begin{aligned}
g_1(t,x) = {} & \beta(t,\ 0.7)g(0,x) + \frac{(1.700\times10^{-3})t\sqrt{d}}{k^{3/2}}\left\{1.233\frac{\sqrt{d}}{k^{1/2}} - \frac{3.467}{k^2} - \frac{273}{k^4} - \frac{78933\kappa}{k^6}\right. \\
& + \left(-\frac{2.237}{k^2} - \frac{133.200}{k^4} + \frac{79631\kappa}{k^6}\right)\coth\left(2\sqrt{\frac{x}{\nu}}\right) \\
& + \left(-\frac{0.102}{k^2} + \frac{173.700}{k^4} + \frac{14681\kappa}{k^6}\right)\coth\left(4\sqrt{\frac{x}{\nu}}\right) \\
& \left. + \left(\frac{0.372}{k^2} - \frac{13.730}{k^4} + \frac{476\kappa}{k^6}\right)\coth\left(6\sqrt{\frac{x}{\nu}}\right)\right\}\tanh^6\left(\sqrt{\frac{x}{\nu}}\right)\tanh\left(\sqrt{\frac{x}{\nu}}\right).
\end{aligned} \tag{58}$$

This result nearly resembles to the one obtained in the work published in [14, 15] that used technique such as Adomian decomposition method. For the classical integer Newton calculus $\gamma = 1$, the terms can be computed using similar iterative approach and get the function g(x,t) to take the form

$$g(t,x) = \sqrt{\frac{17\eta}{\nu}} \tanh^2 \left(\frac{1}{k} \left(x - \frac{\sqrt{d}}{k^{5/2}} t \right) \right) \tag{59}$$

Now we can perform numerical simulations as shown by Figs. 13 to 21 where we have used different expressions of the initial input $g(0,x)$ and considered various values of the fractal-fractional parameter γ. In Fig. 13 and the zoomed-in version (Figs. 14-15), plotted for the initial input $g(0,x) = \sqrt{\frac{17\eta}{\nu}} \tanh^2 \left(\sqrt{\frac{x}{\nu}} \right)$ shows the dynamics of the higher order traveling wave when γ takes the values $\{1,\ 0.9,\ 0.7,\ 0.6,\ 0.5,\ 0.45\}$. We observed the evolution of the higher order traveling wave involved in a self replication process. There is generation of the exact or approximately exact copies of the initial traveling wave in different scales and where the fractal process produces other multiple traveling waves that look like the preceding ones. Hence, the whole replication dynamics incur the influence of both the fractal dimension involved in the system and the fractional parameter which is also the derivative order of the model. The self replication increases and expands as the parameter γ changes in values. A nearly similar dynamic is globally shown in Fig. 16 and the zoomed-in version (Figs. 17- 18), plotted for the initial input $g(0,x) = \sqrt{\frac{17\eta}{\nu}} \sinh^2 \left(\sqrt{\frac{x}{\nu}} \right)$ and when γ takes the values $\{1,\ 0.9,\ 0.7,\ 0.6,\ 0.5,\ 0.45\}$. The same observation is done in Figs. 19, 20 and 21 plotted respectively for the initial inputs $g(0,x) = \sqrt{\frac{17\eta}{\nu}} \cosh^2 \left(\frac{x}{\nu} \right)$, $g(0,x) = \sqrt{\frac{17\eta}{\nu}} \sinh^2 \left(\frac{x}{\nu} \right)$ and $g(0,x) = \sqrt{\frac{17\eta}{\nu}} \tanh^2 \left(\sqrt{\frac{x}{\nu}} \right)$ and when γ takes the values $\{1,\ 0.9,\ 0.7,\ 0.6\}$. Whence, the fractal dynamics for traveling waves of a higher order represent the main results of this paper and are reflected by the graphical simulations in the figures mentioned above. The whole process is shown to be clearly perturbed by both the fractal and fractional dimension of the model.

For $\gamma = 0.9$				
Time (t)	Spatial (x)	Exact value	Numerical value	Error made
0.5	-25	0.000098126	0.000224130	1.26×10^{-4}
	-15	0.036620000	0.036514000	1.06×10^{-4}
	0	0.001372300	0.001470000	1.00×10^{-4}
	15	0.070555000	0.069355000	1.20×10^{-3}
	25.0	0.000118180	0.000120180	2.00×10^{-6}
1	-25	0.000091592	0.000284080	1.20×10^{-4}
	-15	0.034779000	0.034779000	00
	0	0.001390000	0.001380000	1.00×10^{-5}
	15	0.075546000	0.071755000	1.20×10^{-4}
	25	0.000126620	0.000073380	2.00×10^{-4}
1.5	-25	0.000081235	0.000181240	1.00×10^{-4}
	-15	0.048620000	0.069620000	2.10×10^{-2}
	0	0.001410000	0.001510000	1.01×10^{-4}
	15	0.025083000	0.024954000	1.29×10^{-4}
	25	0.000142760	0.000242760	1.00×10^{-4}
2	-25	0.000065920	0.000132590	1.26×10^{-3}
	-15	0.039495000	0.039495000	00
	0	0.001430000	0.040430000	1.00×10^{-2}
	15	0.104610000	0.102610000	2.00×10^{-3}
	25	0.000175920	0.000175920	00
3	-25	0.000045819	0.000224130	1.26×10^{-3}
	-15	0.027489000	0.038768000	1.6×10^{-3}
	0	0.040400000	0.001400000	1×10^{-2}
	15	0.019720000	0.071755000	1.2×10^{-3}
	25	0.000253100	0.000120180	1.01×10^{-5}
4	-25	0.000038771	0.000224130	1.26×10^{-4}
	-15	0.023272000	0.038768000	1.06×10^{-3}
	0	0.040402000	0.041402000	1×10^{-3}
	15	0.026380000	0.026380000	00
	25	0.000299110	0.00012018	2.1×10^{-5}

Table 1: Some values for numerical and exact solutions to the model (53) at $k = 2.5$, $d = 4.0$, and $\gamma = 0.9$.

For $\gamma = 0.7$				
Time (t)	Spatial (x)	Exact value	Numerical value	Error made
0.5	-25	0.000099315	0.000109420	1.01×10^{-5}
	-15	0.013670000	0.013670000	00
	0	0.013107000	0.013107000	00
	15	0.019718000	0.019718000	00
	25	0.000167700	0.000096770	2.00×10^{-5}
1	-25	0.000091592	0.000088572	3.02×10^{-6}
	-15	0.034779000	0.034779000	00
	0	0.013907000	0.013907000	00
	15	0.075546000	0.075546000	00
	25	0.000126620	0.000026620	1.00×10^{-4}
1.5	-25	0.000077901	0.000237900	1.60×10^{-4}
	-15	0.046635000	0.046635000	00
	0	0.012007000	0.012140000	1.31×10^{-4}
	15	0.088688000	0.088688000	00
	25	0.000148870	0.000159170	1.03×10^{-5}
2	-25	0.000056352	0.001316400	1.26×10^{-3}
	-15	0.033785000	0.033785000	00
	0	0.012060000	0.062060000	1.00×10^{-2}
	15	0.022130000	0.020120000	2.01×10^{-3}
	25	0.000205790	0.000205790	00
3	-25	0.000029488	0.001289500	1.26×10^{-3}
	-15	0.017711000	0.019311000	1.6×10^{-3}
	0	0.012060000	0.062060000	1×10^{-2}
	15	0.020430000	0.021630000	1.2×10^{-3}
	25	0.000393270	0.000403370	1.01×10^{-5}
4	-25	0.000021331	0.000020071	1.26×10^{-6}
	-15	0.012819000	0.012830000	1.06×10^{-5}
	0	0.061760000	0.062760000	1.00×10^{-3}
	15	0.005320000	0.005320000	00
	25	0.000543640	0.000543640	00

Table 2: Some values for numerical and exact solutions to the model (53) at $k = 2.5$, $d = 4.0$, and $\gamma = 0.7$.

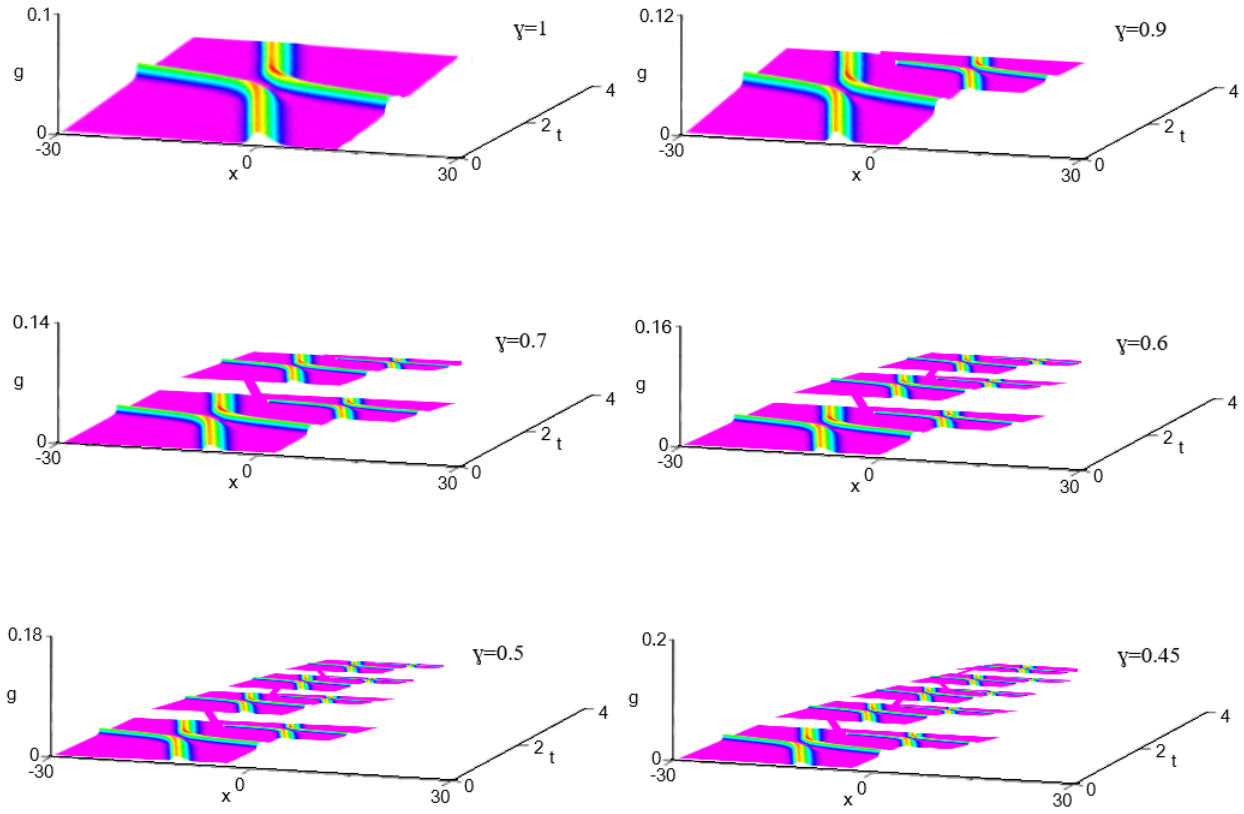

Fig. 13: Numerical simulations of the 7th order KdV equation (27), plotted for the initial input $g(0,x) = \sqrt{\frac{17\eta}{\nu}}\tanh^2\left(\sqrt{\frac{x}{\nu}}\right)$ showing the dynamics of the higher order traveling wave when $\gamma =$ 1, 0.9, 0.7, 0.6, 0.5, 0.45. It happens that the evolution of the higher order traveling wave is involved in a self replication process. There is generation of the exact or approximately exact copy of the initial traveling wave where the fractal process produces other multiple traveling waves that look like the preceding ones. The fractal dynamics expand as the parameter γ changes.

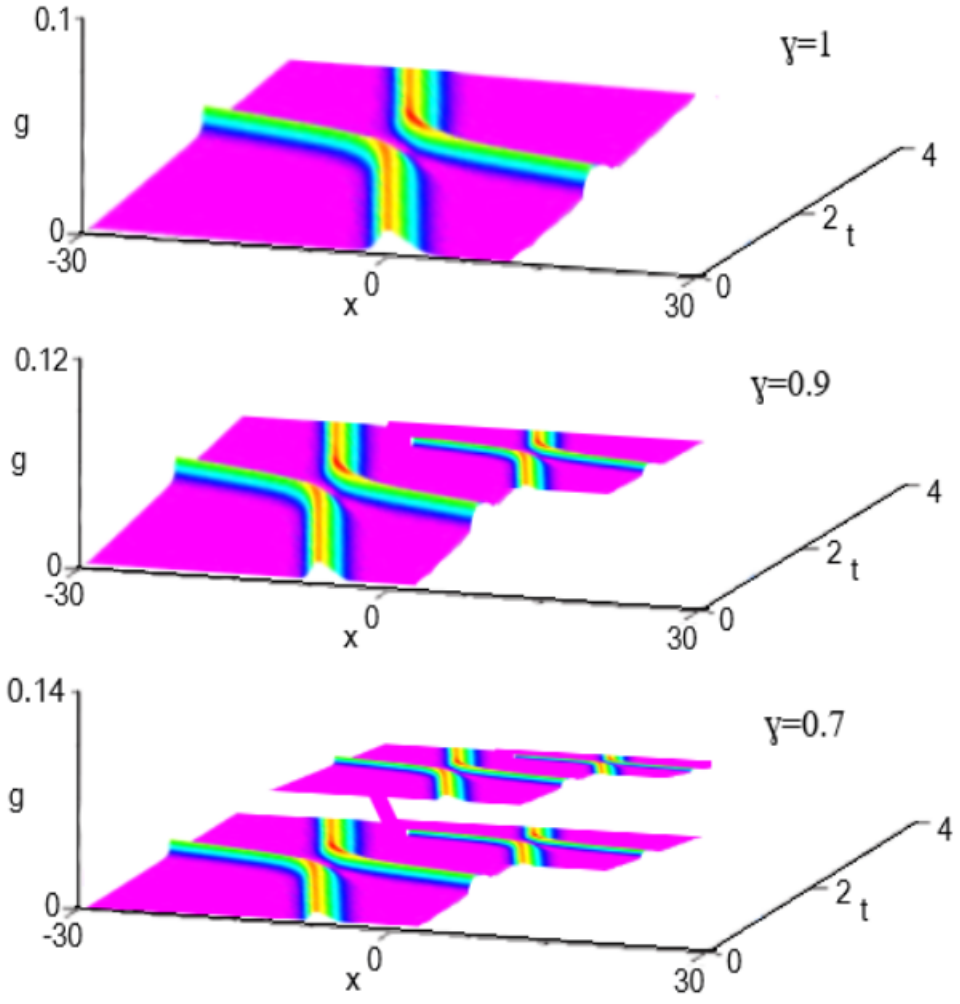

Fig. 14: Enlarged version of Fig. 13 depicting fractal replications performed by the 7th order KdV equation (27), for the initial input $g(0,x) = \sqrt{\frac{17\eta}{\nu}}\tanh^2\left(\sqrt{\frac{x}{\nu}}\right)$ and $\gamma = 1,\ 0.9,\ 0.7,\ 0.6,\ 0.5,\ 0.45$. The fractal dynamics expand as the parameter γ changes.

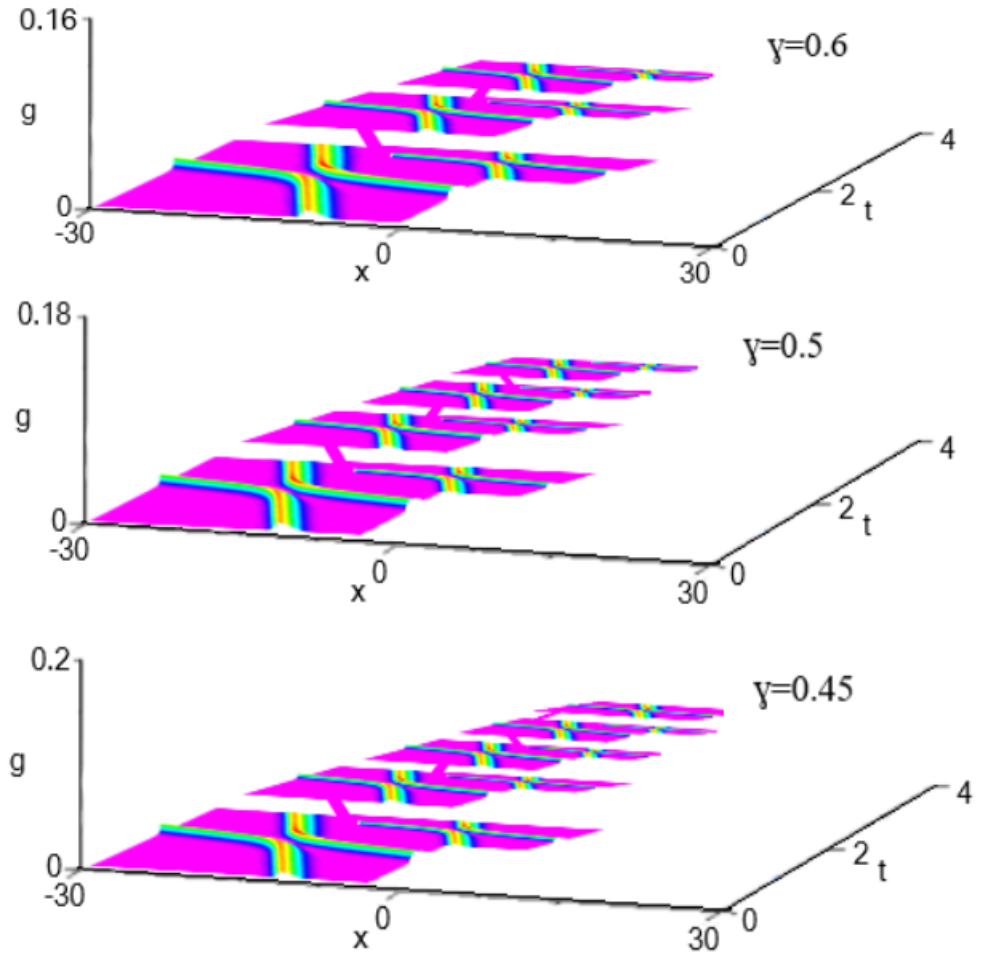

Fig. 15: Enlarged version of Fig. 13 depicting fractal replications performed by the 7th order KdV equation (27), for the initial input $g(0,x) = \sqrt{\frac{17\eta}{\nu}}\tanh^2\left(\sqrt{\frac{x}{\nu}}\right)$ and $\gamma = 1,\ 0.9,\ 0.7,\ 0.6,\ 0.5,\ 0.45$. The fractal dynamics expand as the parameter γ changes.

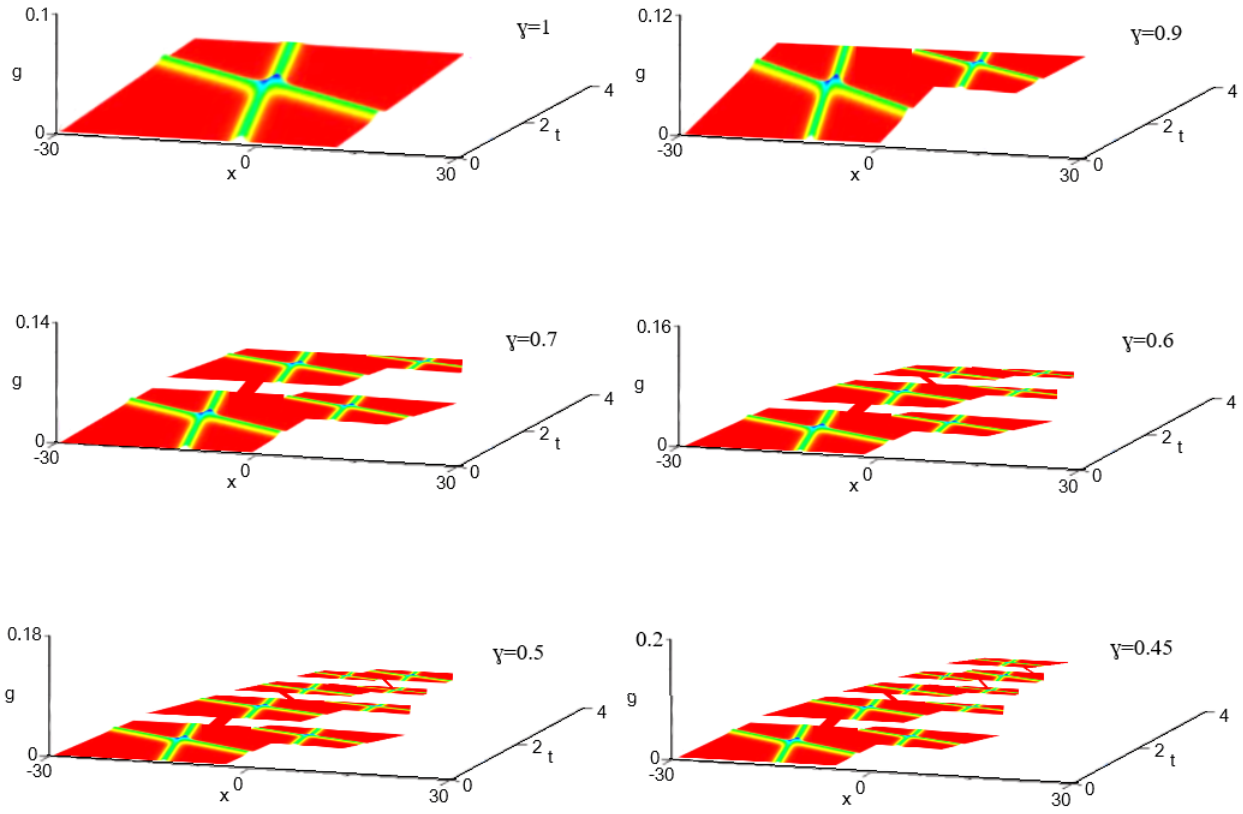

Fig. 16: Numerical simulations of the 7th order KdV equation (27), plotted for the initial input $g(0,x) = \sqrt{\frac{17\eta}{\nu}}\sinh^2\left(\sqrt{\frac{x}{\nu}}\right)$ showing the dynamics of the higher order traveling wave when $\gamma = 1,\ 0.9,\ 0.7,\ 0.6,\ 0.5,\ 0.45$. It happens that the evolution of the higher order traveling wave is involved in a self replication process. There is generation of the exact or approximately exact copy of the initial traveling wave where the fractal process produces other multiple traveling waves that look like the preceding ones. The fractal dynamics expand as the parameter γ changes.

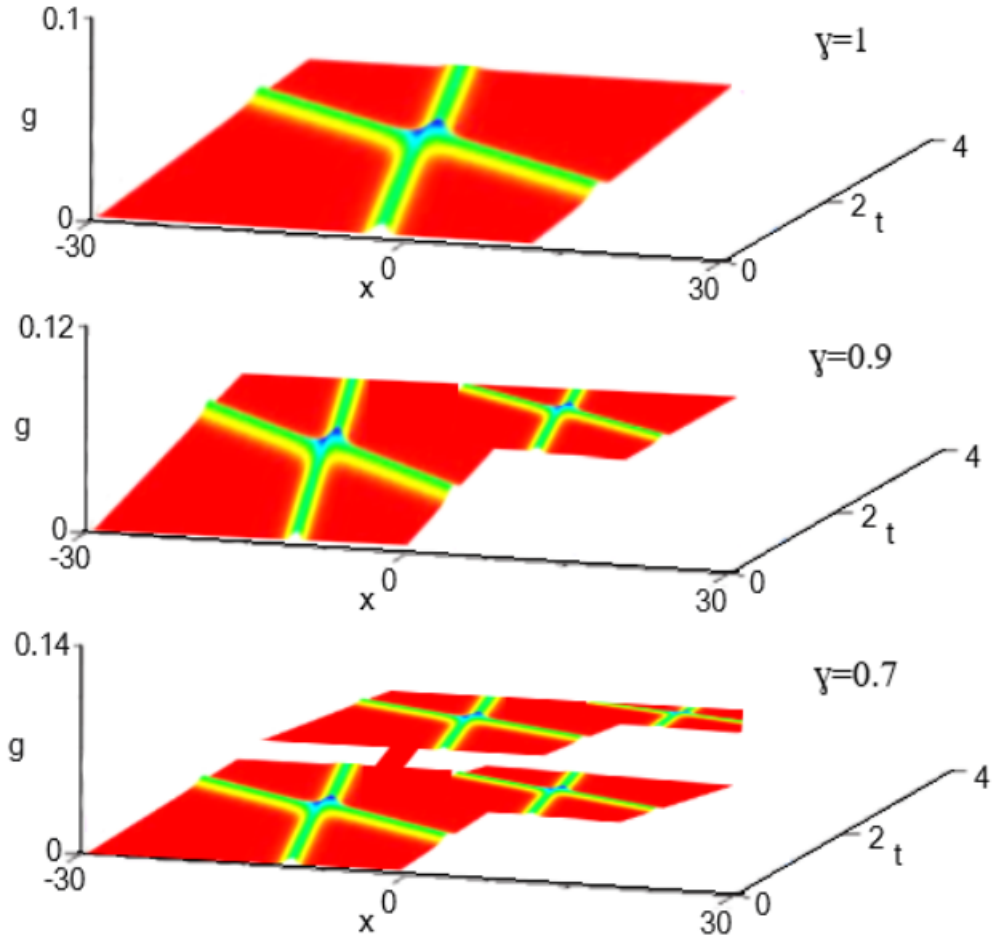

Fig. 17: Enlarged version of Fig. 16 depicting fractal replications performed by the 7th order KdV equation (27), for the initial input $g(0,x) = \sqrt{\frac{17\eta}{\nu}}\sinh^2\left(\sqrt{\frac{x}{\nu}}\right)$ and $\gamma = 1,\ 0.9,\ 0.7,\ 0.6,\ 0.5,\ 0.45$. The fractal dynamics expand as the parameter γ changes.

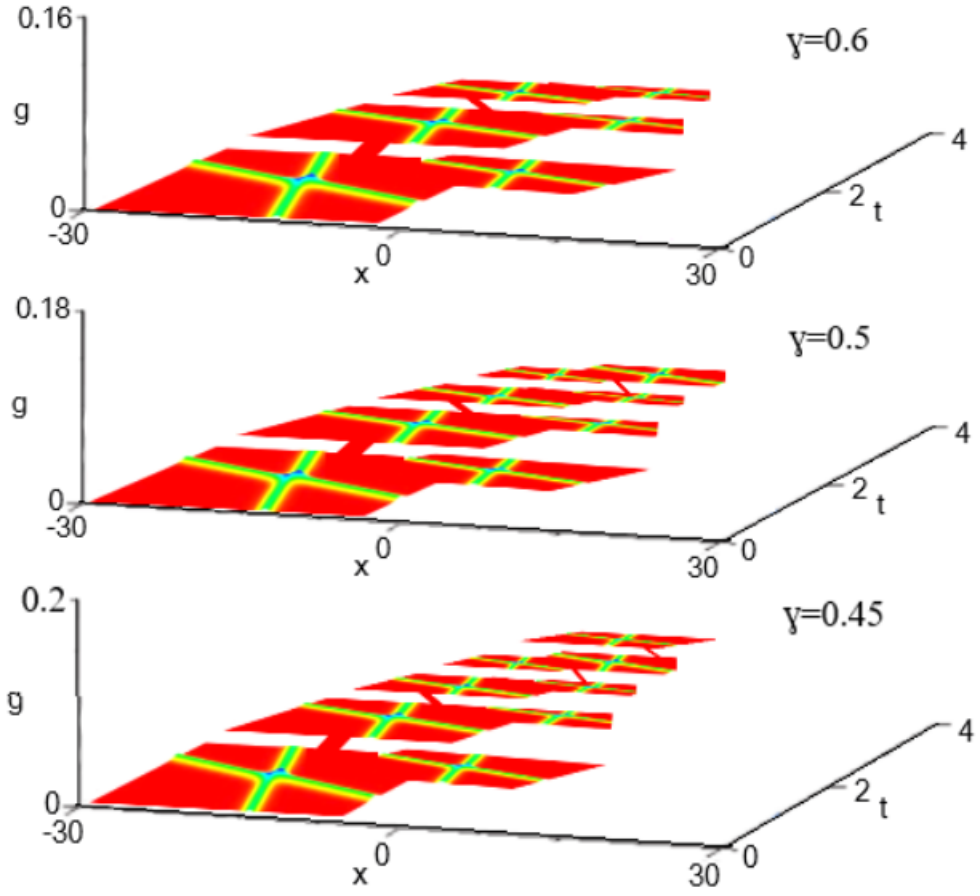

Fig. 18: Enlarged version of Fig. 16 depicting fractal replications performed by the 7th order KdV equation (27), for the initial input $g(0,x) = \sqrt{\frac{17\eta}{\nu}}\sinh^2\left(\sqrt{\frac{x}{\nu}}\right)$ and $\gamma = 1,\ 0.9,\ 0.7,\ 0.6,\ 0.5,\ 0.45$. The fractal dynamics expand as the parameter γ changes.

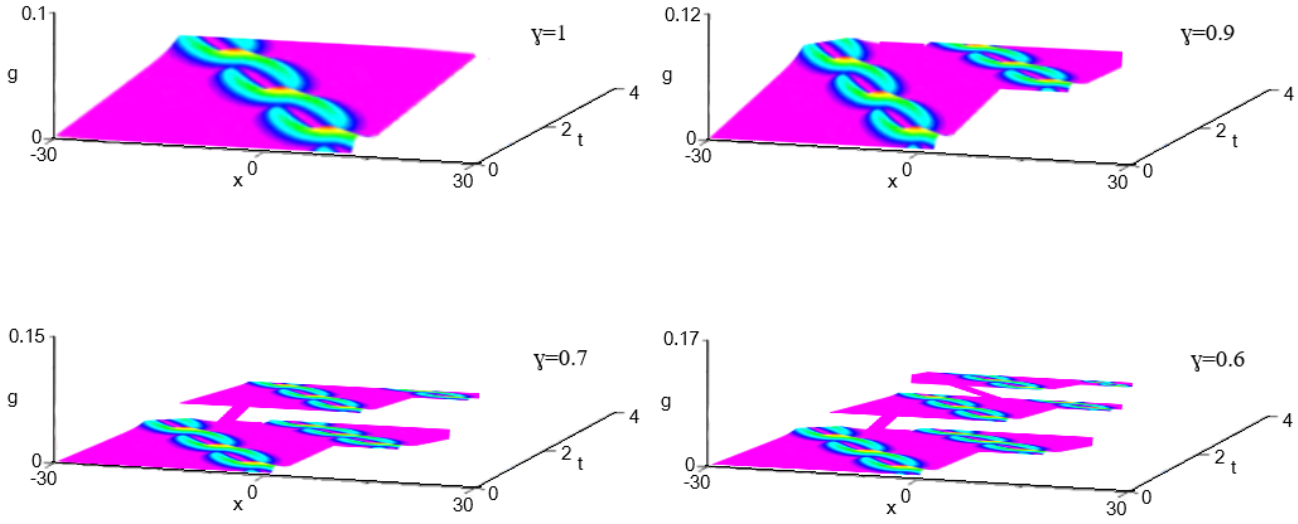

Fig. 19: Numerical simulations of the 7th order KdV equation (27), plotted for the initial input $g(0,x) = \sqrt{\frac{17\eta}{\nu}}\cosh^2\left(\frac{x}{\nu}\right)$ showing the dynamics of the higher order traveling wave when $\gamma = 1,\ 0.9,\ 0.7,\ 0.6$. It happens that the evolution of the higher order traveling wave is involved in a self replication process. There is generation of the exact or approximately exact copy of the initial traveling wave where the fractal process produces other multiple traveling waves that look like the preceding ones. The fractal dynamics expand as the parameter γ changes.

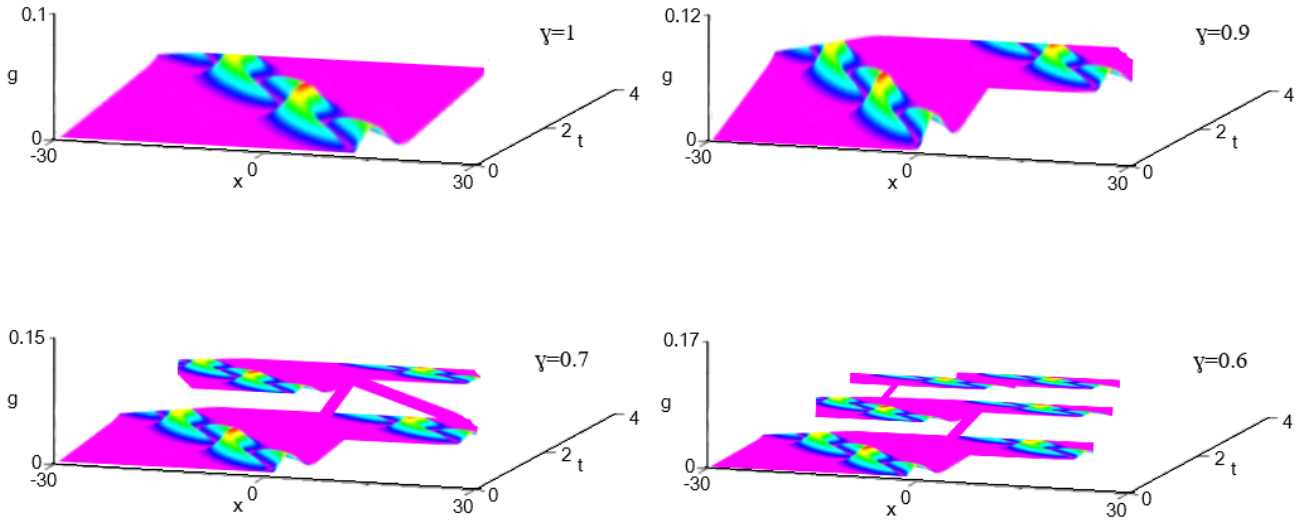

Fig. 20: Numerical simulations of the 7th order KdV equation (27), plotted for the initial input $g(0,x)=\sqrt{\frac{17\eta}{\nu}}\sinh^2\left(\frac{x}{\nu}\right)$ showing the dynamics of the higher order traveling wave when $\gamma=1$, 0.9, 0.7, 0.6. It happens that the evolution of the higher order traveling wave is involved in a self replication process. There is generation of the exact or approximately exact copy of the initial traveling wave where the fractal process produces other multiple traveling waves that look like the preceding ones. The fractal dynamics expand as the parameter γ changes.

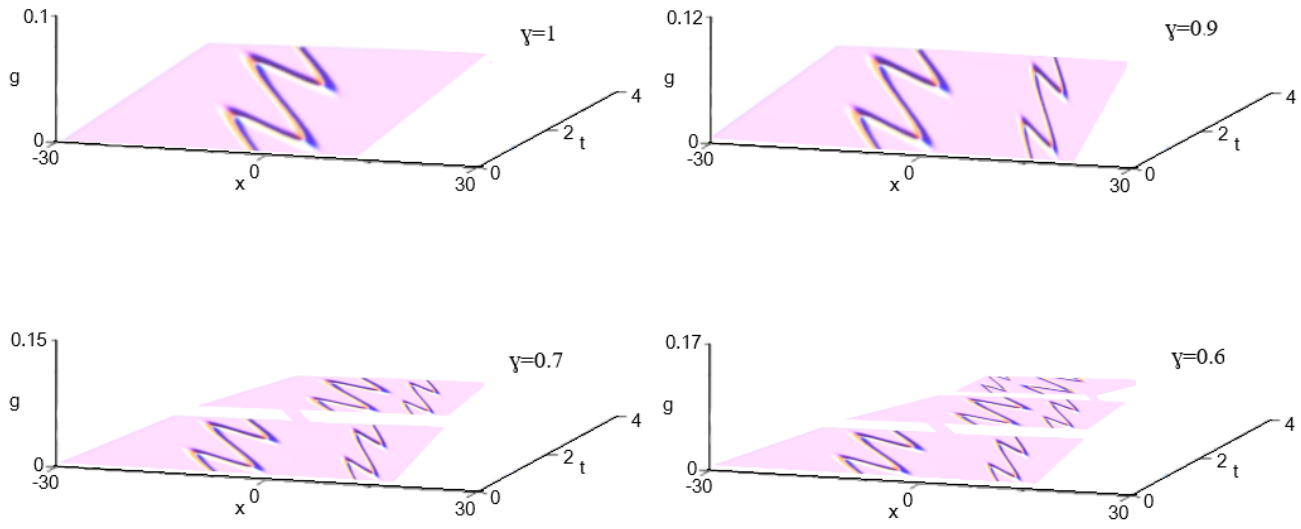

Fig. 21: Numerical simulations of the 7th order KdV equation (27), plotted for the initial input $g(0,x) = \sqrt{\frac{17\eta}{\nu}}\tanh^2\left(\frac{x}{\nu}\right)$ showing the dynamics of the higher order traveling wave when $\gamma = 1,\ 0.9,\ 0.7,\ 0.6$. It happens that the evolution of the higher order traveling wave is involved in a self replication process. There is generation of the exact or approximately exact copy of the initial traveling wave where the fractal process produces other multiple traveling waves that look like the preceding ones. The fractal dynamics expand as the parameter γ changes.

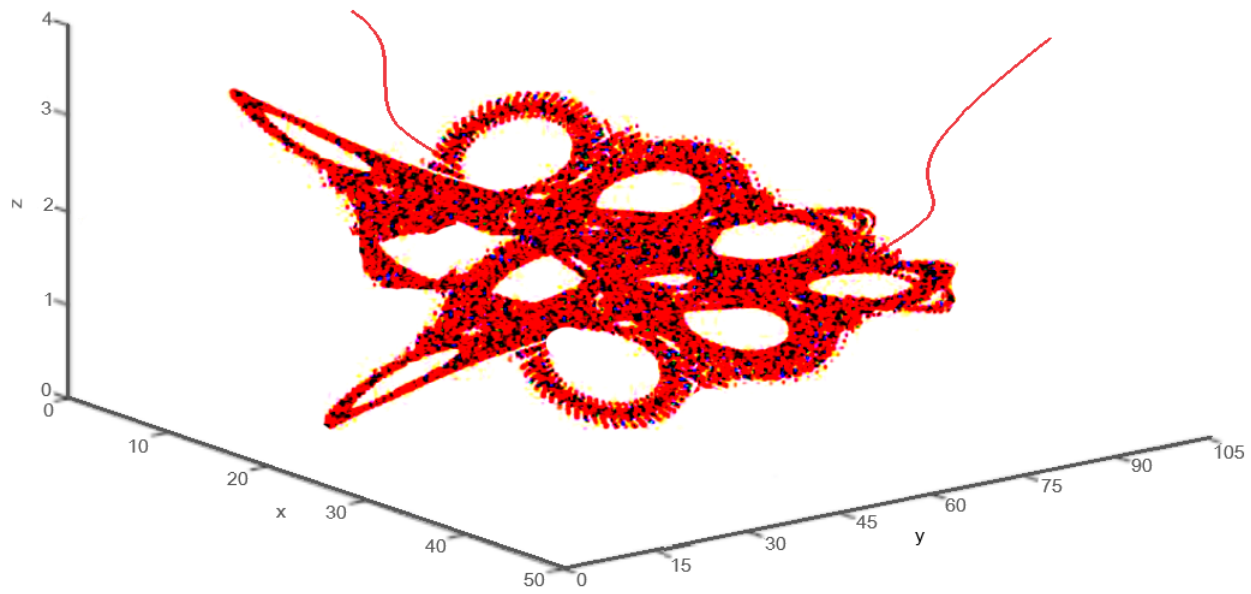

Fig. 22: The superposed roads mapping system representing the model (60)-(61) for $\gamma = 0.9$ and $x(0) = \tilde{x}(x) = 0.2,\ y(0) = \tilde{y}(y) = 0.02,\ z(0) = \tilde{z}(z) = 0.01$. The other parameters used are $a = 34,\ b = 1,\ c = 5$.

4.1 Application 2: The three-dimentional fractal in Dubai superposed roads mapping system

We perform another application by combining the Definition 23 to the three-dimensional superposed roads mapping system proposed in [16] to get

$$\begin{cases} {}^{FRm}D_t^{\gamma} x(t) = y - \text{sign}(x)\sin\left(\log|bx-c|\right)\arctan\left((cx-b)^2\right), \\ {}^{FRm}D_t^{\gamma} y(t) = a - x, \\ {}^{FRm}D_t^{\gamma} z(t) = \text{sign}(z)xy - \frac{1}{10}z + x, \end{cases} \tag{60}$$

with the following initial conditions:

$$x(0) = \tilde{x}(x),\ y(0) = \tilde{y}(y),\ z(0) = \tilde{z}(z). \tag{61}$$

Numerical simulations of model (60)-(61) are shown in Fig. 22 to Fig. 25 which, again, show the three-dimensional fractal structures of the superposed roads mapping system to be in a self-replication process with the influence of the fractional derivative that extends the self-replication in number and shape as the derivative order varies.

4.2 Application 3: Rock fracture

Recall that rock fracture, whether it occurs naturally or caused by humans, and resulting fragments/dust were shown to be one of the major protagonists in the fight against greenhouse gas emission and global warming [17–19]. Seeking to better understand the

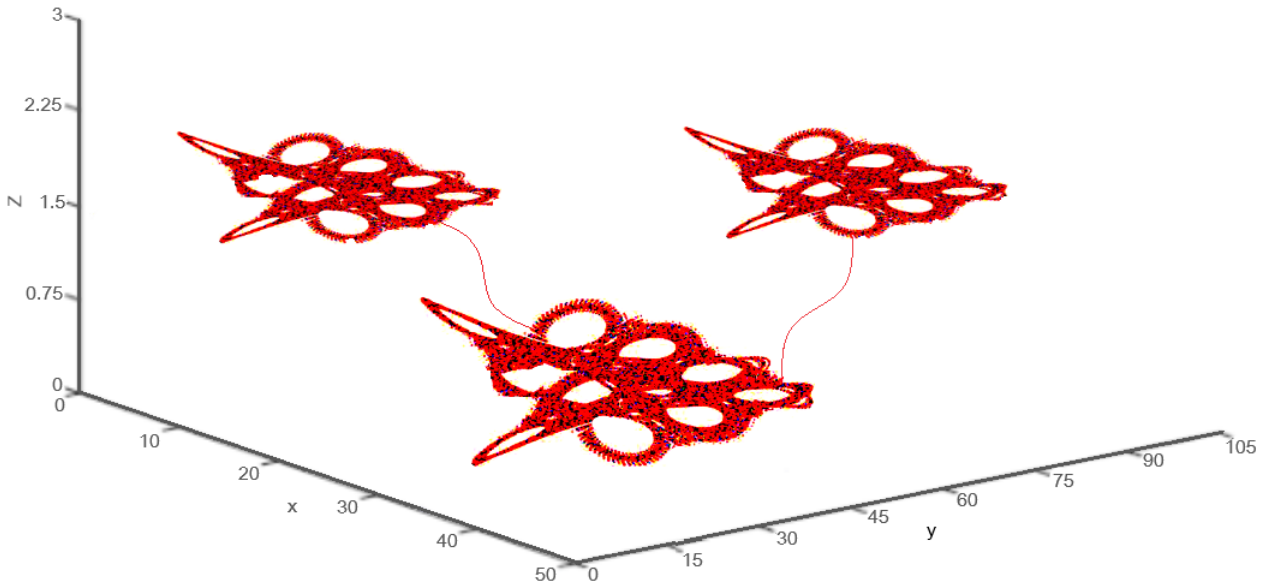

Fig. 23: Representation of model (60)-(61) for $\gamma = 0.8$ and $x(0) = \tilde{x}(x) = 0.2,\ y(0) = \tilde{y}(y) = 0.02,\ z(0) = \tilde{z}(z) = 0.01$. The other parameters used are $a = 34,\ b = 1,\ c = 5$. The dynamics show three-dimensional fractal structures in a self-replication process with the influence of the fractional derivative that extends the self-replication in number and shape as the derivative order varies.

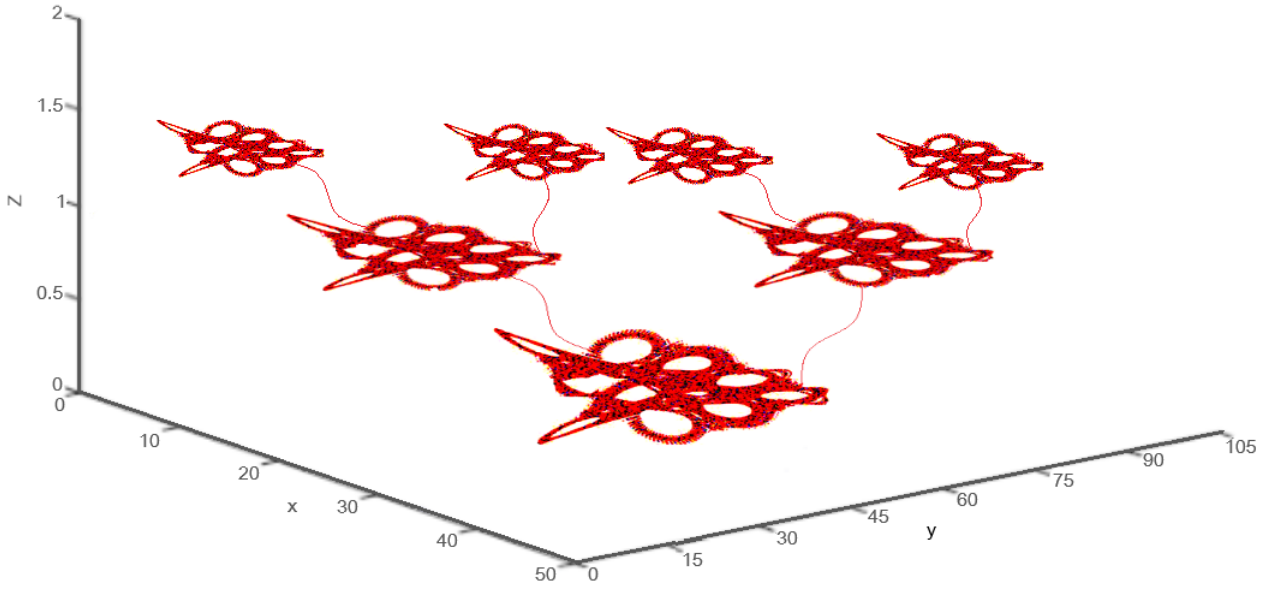

Fig. 24: Representation of model (60)-(61) for $\gamma = 0.6$ and $x(0) = \tilde{x}(x) = 0.2,\ y(0) = \tilde{y}(y) = 0.02,\ z(0) = \tilde{z}(z) = 0.01$. The other parameters used are $a = 34,\ b = 1,\ c = 5$. The dynamics show three-dimensional fractal structures in a self-replication process with the influence of the fractional derivative that further extends the self-replication in number and shape as the derivative order varies

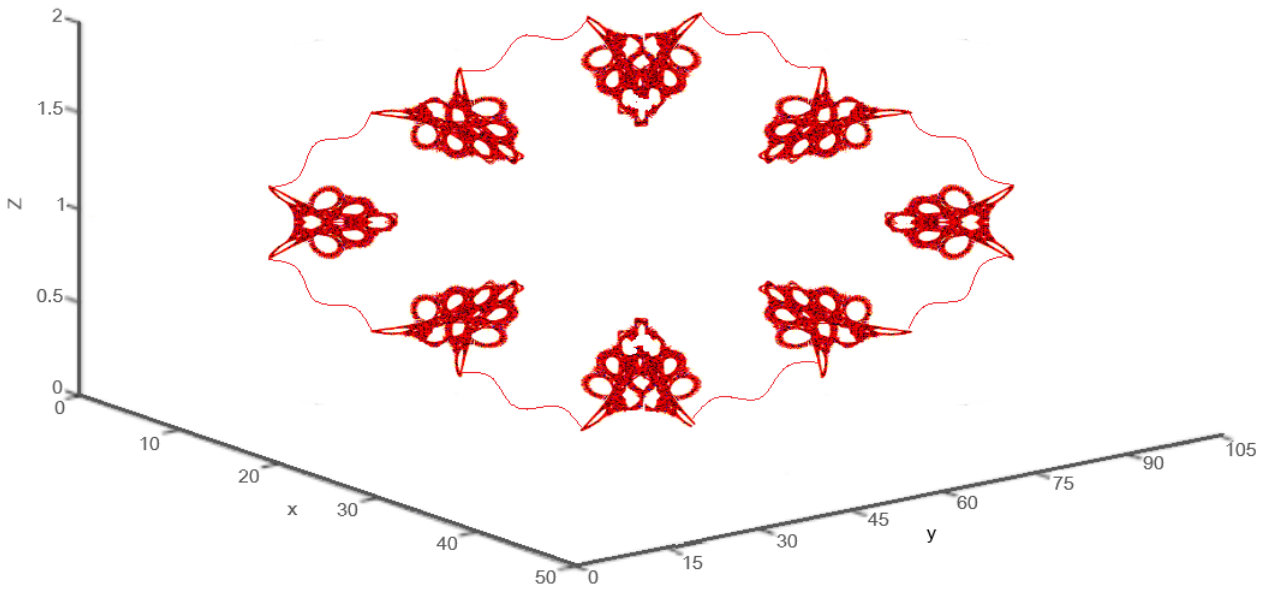

Fig. 25: Representation of model (60)-(61) for $\gamma = 0.4$ and $x(0) = \tilde{x}(x) = 0.2$, $y(0) = \tilde{y}(y) = 0.02$, $z(0) = \tilde{z}(z) = 0.01$. The other parameters used are $a = 34$, $b = -2$, $c = -5$. The dynamics show three-dimensional fractal structures in a self-replication process with the influence of the fractional derivative that further extends the self-replication in number and shape as the derivative order varies

core underlying the rock fracture processes is therefore, more than essential for our planet. The Newton operator dW/dt used in shattering phenomena describes the rate at which there is (mass) loss or accumulation in the process [20, 21]. In other words, it is used, at an infinitesimal and bounded space, to get the difference between gain and loss rates. If we assume that the bounded space contains singularities such as trapdoors of different categories which temporarily keep the main system's variable, then the Newton operator dW/dt will not correctly and accurately describe the accumulation made or loss incurred by the system. Moreover, those singularities may take the form of islands, isolated regions or prohibitive zones where it is impossible for the main variable to belong. This reinforces the idea that the accumulation made or loss incurred by the system cannot be given by the classical Newton operator. This observation represents one of motivations that helped researchers to generalize the classical Newton operator dW/dt into the form $\mathcal{D}^{\gamma} = \partial^{\gamma} W/(\partial t^{\gamma})$, with γ a real or complex number. We continue in the same direction with the model

$$^{FRe}D_t^{\gamma} W(t,x) = -W(x,t)\int_0^x F_{\gamma}(\varrho, x-\varrho)d\varrho + 2\int_x^{\infty} W(\varrho,t)F_{\gamma}(x,\varrho-x)d\varrho, \tag{62}$$

with the condition that the following relation holds

$$W(0,x) = W_0(x). \tag{63}$$

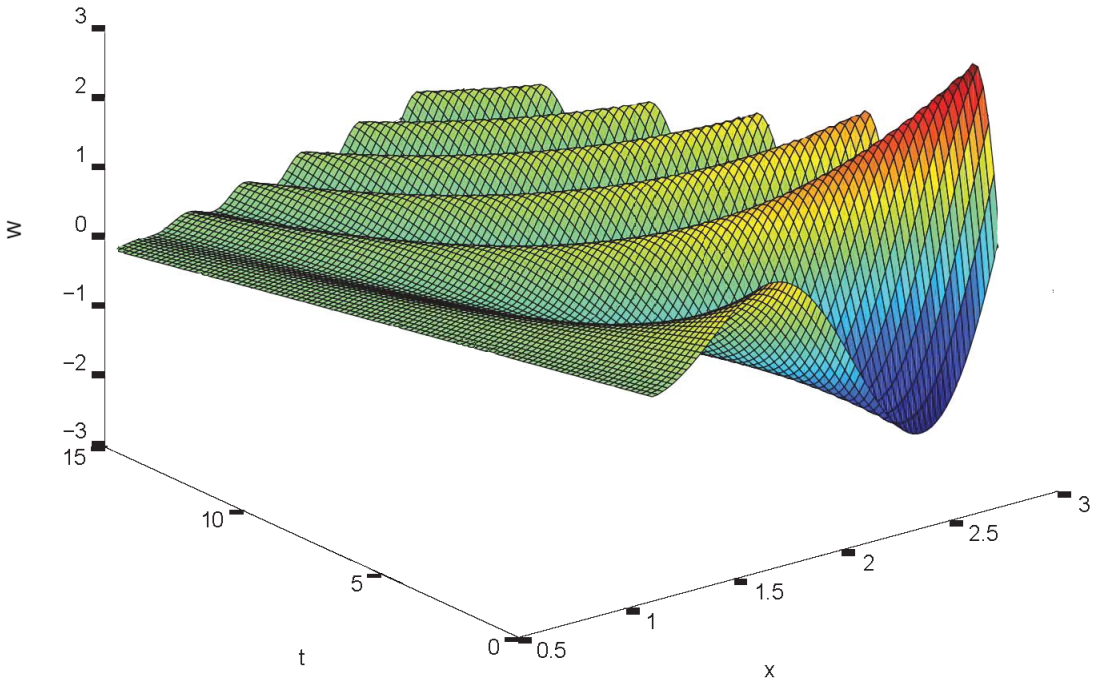

Fig. 26: Three-dimensional representation of the surface solution $W(t,x)$ when $\gamma=1$ and $W_0=\frac{\ln x}{(x^2+2)^2}$

where ${}^{FRe}D_t^{\gamma}$ is the Riemann-Liouville sense operator with the exponential kernel. The three-dimensional representation of the surface solution $W(t,x)$ with $\gamma=1$ and $W_0=\frac{\ln x}{(x^2+2)^2}$ is shown in Fig. 26, followed by appearance of a self-replicated zone that varies as the derivative order γ changes (Fig. 27, Fig. 28) for $\gamma=0.9$ $\gamma=0.65$ and $\gamma=0.55$ respectively).

4.3 Application 4: Merged-Basin of Attraction

We can use the control technique combined to two different concepts, Julia's process and fractal-fractional operator, to generate auto-replication in systems of chaotic attractors with two and three merged basins of attraction. The systems used here comprise a controller part, namely the switching-manifold control. Hence, the model reads as

$$ {}^{FF}D\nu_t X(t)=MX(t)+C_2(X(t)) \tag{64}$$

where we recall that

$$X(t)=\begin{pmatrix} x(t)\\ y(t)\\ z(t)\end{pmatrix} \quad \text{and} \quad M=\begin{pmatrix} a & b & 0\\ -b & a & 0\\ 0 & 0 & c\end{pmatrix}$$

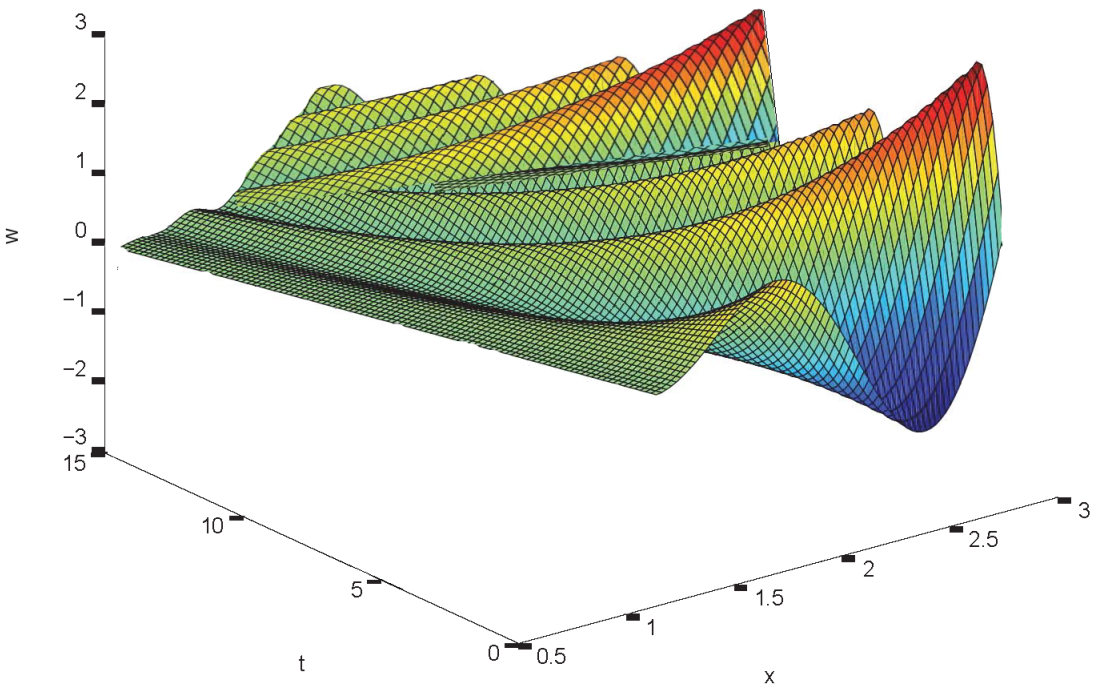

Fig. 27: Three-dimensional representation of the surface solution $W(t,x)$ when $\gamma = 0.9$ and $W_0 = \frac{\ln x}{(x^2+2)^2}$. It shows a dynamic partly repeating itself twice, marking the existence of a self-replicated zone in the rock fracture model that also happens to be chaotic.

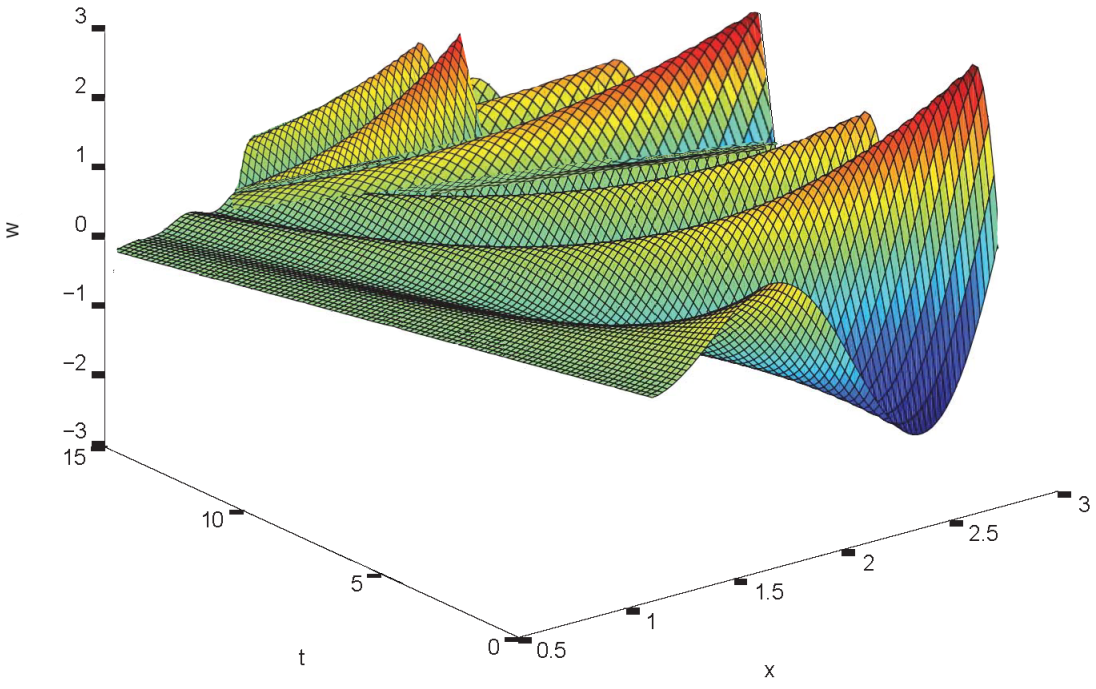

Fig. 28: Three-dimensional representation of the surface solution $W(t,x)$ when $\gamma = 0.65$ and $W_0 = \frac{\ln x}{(x^2+2)^2}$. It shows a dynamic repeating itself three times, marking the existence of a self-replicated zones in the rock fracture model that also happen to be chaotic.

and also

$$C_2(X)=\begin{cases} p\begin{pmatrix} -x(t) \\ -y(t) \\ e_1 \end{pmatrix} & \text{when } z>0 \text{ and } \ p<(x^2+y^2)^{1/2}+z, \\ q\begin{pmatrix} -x(t) \\ -y(t) \\ e_2 \end{pmatrix} & \text{when } z<0 \text{ and } \ -q>-(x^2+y^2)^{1/2}+z, \\ r\begin{pmatrix} 0 \\ 0 \\ -\text{sign(z)} \end{pmatrix} & \text{elsewhere.} \end{cases}$$

1. For $z>0$ and $p<(x^2+y^2)^{1/2}+z$ model (64) reads as

$$\begin{cases} {}^{FF}D\nu_t x(t) &= ax(t)+by(t)-px(t), \\ {}^{FF}D\nu_t y(t) &= -bx(t)+ay(t)-py(t), \\ {}^{FF}D\nu_t z(t) &= cz(t)+pe_1. \end{cases} \tag{65}$$

In order to adequately solve this combined system, we are forced to add the initial conditions given as follows:

$$x(0)=\tilde{x}(x),\ y(0)=\tilde{y}(y),\ z(0)=\tilde{z}(z). \tag{66}$$

The numerical illustrations, after using the Legendre wavelet scheme, are shown in Fig. 29 to Fig. 31 where the system (64) is involved in auto-replication dynamics. They show the generations of chaotic attractor that auto-replicates three times and that possesses two merged basins of attraction consisting of lower and upper basin.

4.4 Application 5: Hindmarsh and Rose neuron 3D-model

Studying & understanding the bursting dynamics of membrane potential in neurobiology is captivating in applied sciences, with many features still to be uncovered. We have analyzed the 3D neuronal activities given by model of Hindmarsh-Rose (HR) neurons with external current input using Haar wavelet method. The analysis considers two control parameters: the external current I^{ext} and the derivative order γ, on top of the other seven usual parameters a,b,c,d,ν_1,ν_2 and x_{rest}. Hence, the 3D model, developed in its generalized form reads as

$$\begin{cases} D_t^\gamma x(t)=I^{\text{ext}}+x^2(b-ax)+y-z, \\ D_t^\gamma y(t)=c-dx^2-y, \\ D_t^\gamma z(t)=\nu x-\nu x_{\text{rest}}-\nu_1 z, \end{cases} \tag{67}$$

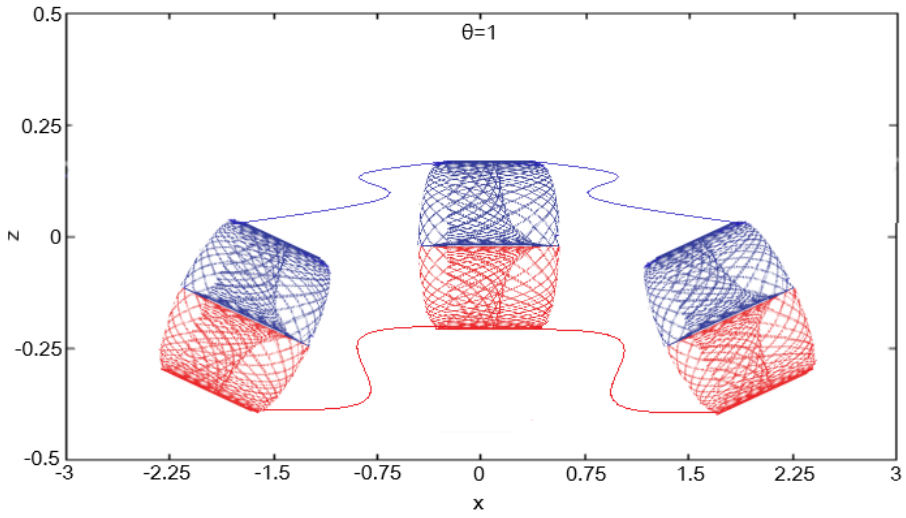

Fig. 29: Illustration of the auto-replication dynamics of the model (64) using the Legendre wavelets scheme. It results in the generations of chaotic attractor that auto-replicates three times and that possesses two merged basins of attraction consisting of lower and a upper basin, joint together at $z=0$. The axis $z=0$ initially plays the role of an axis of symmetry for the attractor viewed on this $(x,z)-$plane. The parameter values used are $(a,b,c)=(3,20,-20)$, $(p,q,r)=(4,4,1)$ and $e_1=e_2=8$.

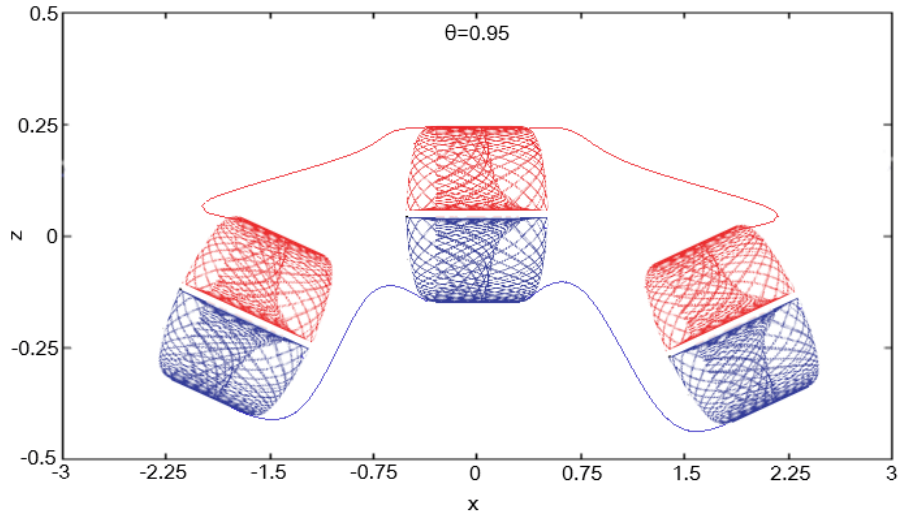

Fig. 30: Illustration of the auto-replication dynamics of the model (64) using the Legendre wavelets scheme. It results in the generations of chaotic attractor that auto-replicates three times and that possesses two merged basins of attraction consisting of lower and a upper basin. However, the two merged basins of attraction are shown to slightly move away as the impact of the fractional dynamics $(\nu=0.95)$. The parameter values used are $(a,b,c)=(3,20,-20)$, $(p,q,r)=(4,4,1)$ and $e_1=e_2=8$.

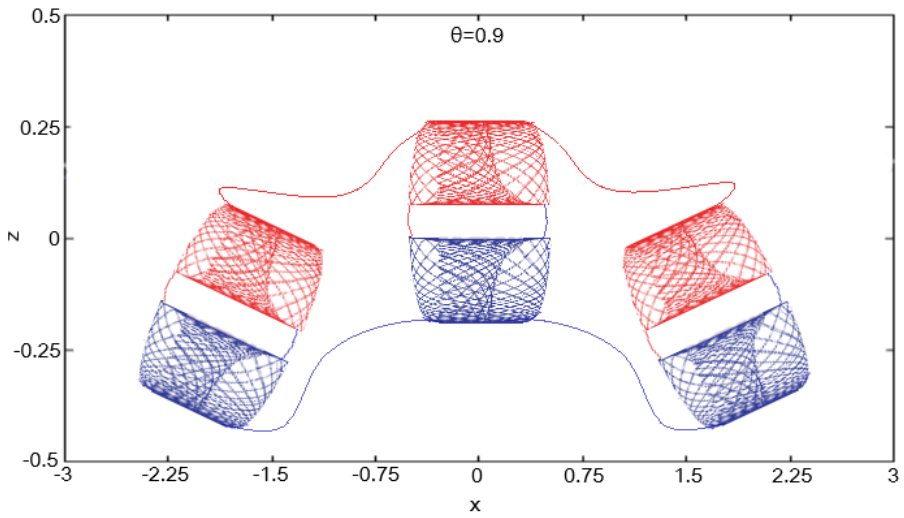

Fig. 31: Illustration of the auto-replication dynamics of the model (64) using the Legendre wavelets scheme. It results in the generations of chaotic attractor that auto-replicates three times and that possesses two merged basins of attraction consisting of lower and a upper basin. However, the two merged basins of attraction are shown to further move away as the impact of the fractional dynamics ($\nu = 0.9$). The parameter values used are $(a,b,c) = (3,20,-20)$, $(p,q,r) = (4,4,1)$ and $e_1 = e_2 = 8$.

with $\nu = \nu_1\nu_2$ and assumed to satisfy the following initial conditions

$$x(0) = f(x),\ y(0) = g(y),\ z(0) = l(z), \tag{68}$$

where the variable $x = x(t)$ represents the membrane potential, $y = y(t)$ is a recovery variable linked to the fast current of Na^+ or K^+ ions, $z = z(t)$ represents the adaptation current related to the slow current of Ca^{2+} ion. All the four parameters a, b, c, d, usually determined experimentally, are taken to be real numbers. The term D_t^{γ} represents the standard Caputo fractional derivative of order γ, with $0, \gamma \leq 1$.

Numerical representation of solutions to (67)-(68) are depicted Fig. 32 and Fig. 33 for different values of the derivative order γ and for external current $I^{\text{ext}} = 0.5$ and $I^{\text{ext}} = 2.2$ respectively.

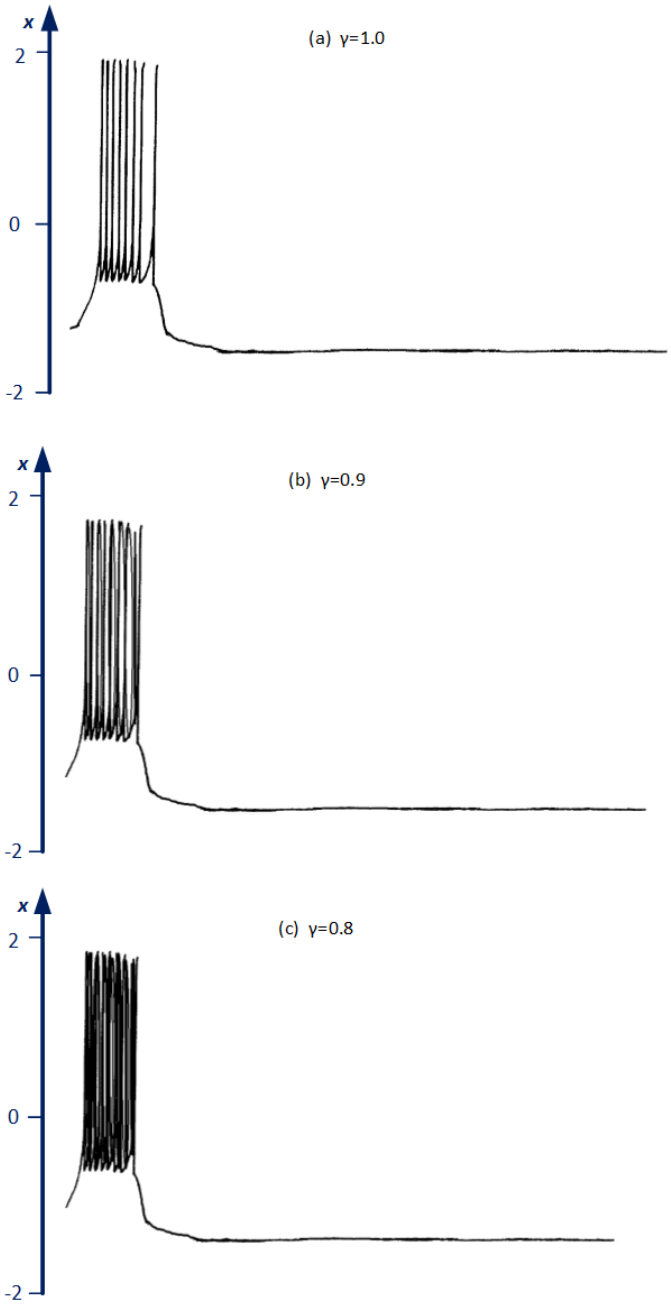

Fig. 32: Numerical solutions showing response of HR neuron 3D-model's membrane potentials for a short current pulse $I = 0.5$ with $a = 1,\ b = 3,\ c = 1,\ d = 5$ and for $\gamma = 1.0,\ 0.9,$ and 0.8 respectively. We observe in all three cases regular isolated burst turning into Period-adding chaotic bifurcation (burst with uncountable peaks) as γ decreases. This hereby gives γ the status of a suitable parameter for the system control.

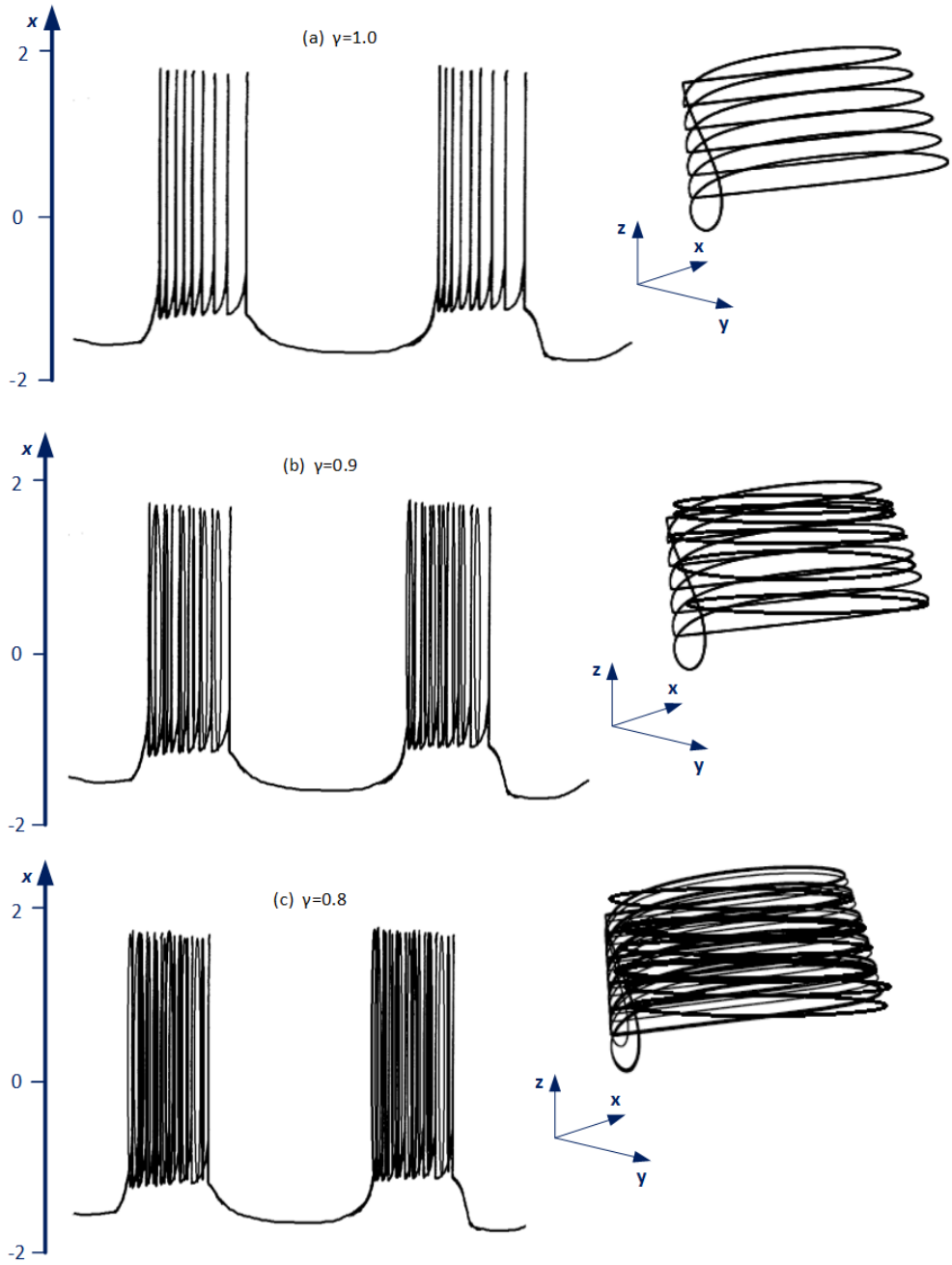

Fig. 33: Numerical solutions showing response of HR neuron 3D-model's membrane potentials for $I = 2.2$ with $a = 1,\ b = 3,\ c = 1,\ d = 5$ and for $\gamma = 1.0,\ 0.9,$ and 0.8 respectively. Similar to Fig. 32, we observe in all three cases regular but non-isolated burst turning again into Period-adding chaotic bifurcation (burst with uncountable peaks) as γ decreases. This chaos is confirmed by the phase representation in the space (x, y, z) (on the right). Furthermore, the sequence of repeated bursts happens faster as γ decreases.

5 conclusion

We have combined in this work some recent mathematical concepts to model and generate some fractal processes happening in real life and useful in applied sciences (chaos theory, wave motion, rock fracture, neuron science). In the analysis process, we have used systems of differential equations together with the fractal and fractional operators, which are derivatives with a fractional order. We have shown the huge and exceptional impacts of these fractal and fractional operators in the different systems of equations used to described numbers of real life processes. The outcomes obtained concur with the expected results as numerical simulations have proved that the new systems are involved in various types of fractal dynamics with the replication of the initial objects and the formation of subsequent fractal patterns which vary with an important parameter of the model: the fractional derivative order. The main prowess here is the proof that differential systems involved in the analysis are able to artificially structure fractals using mathematical concepts, numerical techniques and simulations. These results improve the preceding ones with the combination of recently developed operators to classical models and generate complex patterns used and applied by scientists and engineers.

Acknowledgments:

(a) I am grateful to the Almighty God for his love and protection throughout my career.

(b) Specials thanks go to my immediate family for their unconditional support and encouragement throughout my career; I think of my wife Alexandra, kids Cecilia, Tylio, Louwenn and Yannzi, mother Jeannette Goufo, brother Vivien and sister Hermine.

(c) Foremost tributes also go to my late fathers, Jean-Paul Goufo and Daniel Kenne and late sister Marianne.

(d) I am grateful to my colleagues in the maths department for their continuous support, encouragement and collegiality.

(e) I acknowledge with unfettered and hearty gratitude to people who, one way or the other, had positive influence on my academic career and progress. They are Prof A. Atangana, Prof J. Manale (MSc supervisor), Prof R. Maritz (MSc co-supervisor), Prof CS. Oukouomi Noutchie (PHD supervisor), Prof J. Banasiak (PHD advisor), Prof M. Mbehou, Dr S. Mugisha, Prof S. Kumar, Prof B. Tsanou, Dr I. Tchangou, Dr HM. Tenkam,

(f) Let me also thank my friends here today, A. Charette, Imelda, Alvesia.

(g) Lastly I thank you all for coming and the interest you have shown in my inaugural lecture.

References

[1] M. Caputo and M. Fabrizio, A new definition of fractional derivative without singular kernel, *Progr. Fract. Differ. Appl* **1**(2) (2015) 1–13.

[2] J. Losada and J. J. Nieto, Properties of a new fractional derivative without singular kernel, *Progr. Fract. Differ. Appl* **1**(2) (2015) 87–92.

[3] E. F. D. Goufo and A. Atangana, Analytical and numerical schemes for a derivative with filtering property and no singular kernel with applications to diffusion, *The European Physical Journal Plus* **131**(8) (2016) p. 269.

[4] A. Atangana and D. Baleanu, New fractional derivatives with non-local and non-singular kernel, *Thermal Science* **20**(2) (2016) 763–769.

[5] E. F. Doungmo Goufo, Chaotic processes using the two-parameter derivative with non-singular and non-local kernel: Basic theory and applications, *Chaos: An Interdisciplinary Journal of Nonlinear Science* **26**(8) (2016) p. 084305.

[6] E. D. Goufo, A biomathematical view on the fractional dynamics of cellulose degradation, *Fractional Calculus and Applied Analysis* **18**(3) (2015) 554–564.

[7] E. D. Goufo, A mathematical analysis of fractional fragmentation dynamics with growth, *Journal of Function Spaces* **2014**(1) (2014) p. 7 pages.

[8] I. Podlubny, *Fractional Differential Equations* (Academic Press, New York, 1999).

[9] E. F. D. Goufo and Y. Khan, A new auto-replication in systems of attractors with two and three merged basins of attraction via control, *Communications in Nonlinear Science and Numerical Simulation* (2021) p. 105709.

[10] A. Atangana, Fractal-fractional differentiation and integration: Connecting fractal calculus and fractional calculus to predict complex system, *Chaos, Solitons & Fractals* **102** (2017) 396–406.

[11] E. F. D. Goufo, On the fractal dynamics for higher order traveling waves, *Chaos, Solitons & Fractals* **148** (2021) p. 111059.

[12] E. F. Doungmo Goufo, A biomathematical view on the fractional dynamics of cellulose degradation, *Fractional Calculus and Applied Analysis* **18**(3) (2015) 554–564.

[13] S. Das, *Functional fractional calculus* (Springer Science & Business Media, 2011).

[14] S. M. El-Sayed and D. Kaya, An application of the adm to seven-order sawada–kotara equations, *Applied mathematics and computation* **157**(1) (2004) 93–101.

[15] R.-X. Yao and Z.-B. Li, On t/x-dependent conservation laws of the generalized nth-order kdv equation, *Chinese Journal of Physics* **42**(4) (2004) 315–322.

[16] A. Atangana and T. Mekkaoui, Trinition the complex number with two imaginary parts: fractal, chaos and fractional calculus, *Chaos, Solitons & Fractals* **128** (2019) 366–381.

[17] D. J. Beerling, E. P. Kantzas, M. R. Lomas, P. Wade, R. M. Eufrasio, P. Renforth, B. Sarkar, M. G. Andrews, R. H. James, C. R. Pearce *et al.*, Potential for large-scale co 2 removal via enhanced rock weathering with croplands, *Nature* **583**(7815) (2020) 242–248.

[18] R. Revelle and H. E. Suess, Carbon dioxide exchange between atmosphere and ocean and the question of an increase of atmospheric co2 during the past decades, *Tellus* **9**(1) (1957) 18–27.

[19] M. Ansarizadeh, K. Dodds, O. Gurpinar, U. Kalfa, T. Ramakrishnan, N. Sacuta and S. Whittaker, Carbon dioxidechallenges and opportunities, *Oilfield Review* **27**(2) (2015) 36–50.

[20] W. J. Anderson, *Continuous-time Markov chains: An applications-oriented approach* (Springer Science & Business Media, 2012).

[21] E. F. D. Goufo, Bounded perturbation for evolution equations with a parameter & application to population dynamics, *Discrete & Continuous Dynamical Systems-S* **14**(7) (2021) p. 2137.